

**SMART COOLING OF RESIDENTIAL BUILDING SPACES  
WITH IMPINGING JETS**

**Bakhtiyar Kalzhan, B. Eng**

**Submitted in fulfilment of the requirements**

**for the degree of Master of Science**

**in Mechanical & Aerospace Engineering**



**School of Engineering and Digital Sciences**

**Department of Mechanical & Aerospace Engineering**

**Nazarbayev University**

53 Kabanbay Batyr Avenue,

Nur-Sultan city, Kazakhstan, 010000

**Supervisor:** Luis R. Rojas-Solórzano

**Co-supervisor:** Desmond Adair

**April 2021**

## DECLARATION

I hereby, declare that this manuscript, entitled "Smart Cooling of Residential Buildings with Impinging Jets", is the result of my own work except for quotations and citations which have been duly acknowledged.

I also declare that, to the best of my knowledge and belief, it has not been previously or concurrently submitted, in whole or in part, for any other degree or diploma at Nazarbayev University or any other national or international institution.



-----  
Name: Bakhtiyar Kalzhan

Date: 11.04.2021

## **Abstract**

Nowadays, humankind is facing problems with global energy deficiency and global warming. During hot periods or in hot climate regions people use traditional cooling methods. These methods use energy to cool the whole space and are not energy efficient. To face the problem, the application of impinging jets for direct cooling of occupants was proposed. Numerical investigations were done in Ansys CFX and thermal comfort was measured by the CBE comfort tool. The domain for impinging jets had three jets with the same diameter of 8 cm. One of the jets was normal to the occupant, while the rest were focused on cooling the head, shoulder and waist regions. Results showed that impinging jets can provide thermal comfort and are an energy efficient solution that can save 18.3% of energy.

## **Acknowledgments**

I want to express my gratitude to Professor Luis R. Rojas – Solórzano. He is a person I respect and admire. I deeply appreciate his support throughout the thesis preparation process.

# Table of Contents

<b>Chapter 1 – Introduction .....</b>	<b>5</b>
<b>Chapter 2 – Literature Review .....</b>	<b>7</b>
<b>2.1. Human body thermoregulation and skin temperature .....</b>	<b>7</b>
<b>2.2. Thermal comfort .....</b>	<b>10</b>
<b>2.3. Mechanical ventilation.....</b>	<b>11</b>
<b>2.4. Human geometry in CFD .....</b>	<b>12</b>
<b>2.5. Impinging jets.....</b>	<b>13</b>
<b>2.5.1. Impinging jet regions .....</b>	<b>13</b>
<b>2.5.2. Turbulence generation and effects .....</b>	<b>15</b>
<b>Chapter 3 – Methodology .....</b>	<b>20</b>
<b>3.1. Domain preparation (Verification and Validation) .....</b>	<b>20</b>
<b>3.2. Mesh verification for jets.....</b>	<b>26</b>
<b>Chapter 4 – Results and Discussion .....</b>	<b>28</b>
<b>4.1. Base case scenario (mixing ventilation cooling) .....</b>	<b>28</b>
<b>4.2. Cooling with impinging jets .....</b>	<b>31</b>
<b>4.3. Energy consumption comparison .....</b>	<b>34</b>
<b>Chapter 5 – Conclusion .....</b>	<b>35</b>
<b>References.....</b>	<b>36</b>
<b>Appendix A .....</b>	<b>40</b>

## Chapter 1 – Introduction

People must live in comfortable conditions because it impacts an individual's health, productivity, mood [1]. Unlike other living organisms, human beings can create comfort artificially with technologies' help. According to a study, people spend 90% of their time indoors [2]. In buildings, the thermal balance is determined by occupants' density, activity levels, latent heat loads, heat exchange between outdoors and indoors, and many other factors. The preponderance of some factors results in either overcooling or overheating the space, which creates discomfort and negatively impacts the occupant's performance. In spaces with poor air quality, deterioration of productivity and sick building syndrome were noticed by Seppanen et al. [3]. Tsai et al. [4] and Lan et al. [5] also reported the relationship between thermal discomfort and sick building syndrome.

Accumulated excessive heat and carbon dioxide particles can be taken away by delivering fresh cool air. People use passive or active (mechanical) methods for space cooling. Natural ventilation, which is a type of passive cooling, is solely driven by wind and buoyancy forces, which is considered the simplest way to cool buildings and is used widely. Although natural ventilation does not depend on electricity, it is not practical when the outdoor temperature and humidity rates are higher than the indoors or when the outdoor air quality is poor (dust, unpleasant odors). Noise, privacy, and security concerns cannot be satisfied with opening windows and doors, making mechanical ventilation preferred over natural ventilation. Mechanical ventilation controls the air humidity, temperature, speed, and contaminants coming into the room. Maintaining a comfortable indoor environment with active methods is done by cooling the whole space with appliances that require electricity. On hot days or in regions with a hot climate, these cooling devices operate non-stop throughout the day. In terms of energy consumption, cooling the whole space is not only inefficient but also time-consuming. Nowadays, the world is facing an energy crisis and global warming. The building sector consumes 40% of total energy and produces 30-40% greenhouse emissions [6]. Between 1990 and 2016, space cooling's energy consumption tripled and reached 2020 Terawatt-hours (TWh). During the same period, the demand for electricity used for space cooling went up from 13% to 20% [7]. Predictions done by Santamouris M. show that the need for cooling energy will continue to grow and reach 34% in 2050 and 61% in 2100 [8]. According to the statistics of the Intergovernmental Panel on Climate Change (IPCC), buildings will generate 14.3 gigatonnes of CO<sub>2</sub> by 2030 [9].

In the modern world, people use commercially available electronic devices such as fans, air-conditioners (ACs), evaporative coolers. Among the devices, ACs are the most popular, with 2 billion customers worldwide [10]. Until 1955, ACs were rare and owned only by 2% of Americans. Due to the country's economic development, 50% of the American population was equipped with ACs by 1980 [11]. Many developing countries make up 35% of the people, and only 10% have ACs installed. Among developing countries, a noticeable growth is seen in Indonesia and India, where the ACs purchase rate increased by 13% and 15%, respectively [10].

With the rise of population and improvements in life quality, the cooling demand will only increase. Cooling the whole space with electronic devices requires a tremendous amount of energy. Its continuous waste will worsen the current global warming and energy crisis. Therefore, more efforts should be made on the creation of alternative cooling methods.

Impinging jets have been widely investigated due to their high heat transfer ratio. The high heat removal rate is achieved due to pressurized airflow coming from the jet nozzle with a small diameter. In commerce or industry rapid cooling or heating is important. The application of impinging jets includes cooling of turbine blades, drying of wood/paper, cooling of a grinding process.

This work is an effort to see if impinging jets can be used as an energy-efficient substitute for space cooling, which will also provide thermal comfort for the occupants. The idea is to install impinging jets to the ceiling of a room and cool a person or people solely. Smart cameras sticking to the jets will detect the occupants' presence and movement and direct the cool air accordingly. Another enhancement is that impinging jets can function continuously or intermittently.

## Chapter 2 – Literature Review

### 2.1. Human body thermoregulation and skin temperature

People are biochemical organisms that require food to maintain life. All the consumed food gets digested, and its valuable components get absorbed by cells. Absorbed chemicals transform into energy that is needed to keep organs alive and produce new organic material. This process is known as metabolism, which constantly generates energy [12]. Some portion of the energy is spent or transformed into heat to regulate the body temperature because core organs cannot survive in wide temperature ranges. The core body temperature is kept at around 37°C. Human body thermoregulation is a complicated system regulated by a brain part called the hypothalamus [13]. The produced heat by the body is exchanged with the environment through convection and radiation or lost by sweat evaporation. 25% of heat is dissipated by evaporation and the rest by convection and radiation [14]. Thermal discomfort starts when a human cannot dissipate heat to the surrounding because its temperature is higher than the body temperature or when the ambient temperature is too cold. Therefore, additional thermoregulation mechanisms are triggered to maintain the temperature. These mechanisms are sweating, shivering, vasodilatation, and vasoconstriction. The agents are activated when ambient temperature changes are sensed by the skin. The production of sweat by skin pores allows cooling the body by taking away the heat through convection and evaporation. In winter or cold conditions, shivering occurs, which is a process of muscle contractions to generate heat. Vasodilatation and vasoconstriction are both related to blood vessels. Vasodilation is responsible for blood vessel expansion, while vasoconstriction is its opposite. The dilation of blood vessels is due to vessels' relaxation, which enhances the blood flow leading to the increased body heat dissipation. On the contrary, tightening of blood vessels creates resistance to blood flow, allowing retaining heat [15]. For thermal comfort evaluations, not the core body temperature but the skin temperature must be used as a reference value [14].

The skin contains millions of sensors and nerves and protects us from unfavorable external factors. Information of environmental changes detected by skin sensors is transmitted to the brain, where decisions regarding thermoregulation mechanisms are made. Skin covers approximately 2 m<sup>2</sup> area of the human body [16]. The relation between skin surface area, body height, and body weight were proposed by DuBois and had the following formulation:

$$A_{DuBois} = 0.202M^{0.425}L^{0.725} \quad (1)$$



where  $A_{DuBois}$  is the skin area,  $M$  is the mass, and  $L$  is the height of a person [17]. According to measurements taken from children and adults, the skin surface area ranges between 0.8 and 2.4 m<sup>2</sup> [15]. In neutral conditions, the skin temperature is not uniformly distributed throughout the body, as can be seen in data provided by Zhang H. [18] and Olesen and Fanger [19]. Two datasets show similar temperature distribution; however, Zhang H's results were consistently higher by 1°C due to unknown reasons (Table 1).

**Table 1. Skin temperature distribution at different segments [15].**

Segment	Skin temperature (°C) – UC Berkeley	Skin temperature (°C) – Olesen and Fanger
Forehead	35.8	34.2
Cheek	35.2	
Front neck	35.8	
Back neck	35.4	
Chest	35.1	34.5
Back	35.3	34.4
Abdomen	35.3	34.9
Upper arm	34.2	33.5
Lower arm	34.6	32.7
Hand	34.4	33.5
Left finger	35.3	
Thigh	34.3	33.7
Shin	32.9	32.6
Calf	32.7	32.2
Foot	33.3	32.2
Average	34.45	33.38

In a cold environment, the skin temperature deviates significantly from neutral conditions because vasoconstriction is the most effort to conserve core body temperature. From Table 2, it can be noticed that the skin temperature at fingers and feet has the lowest values of 21.1°C and 21.4°C, respectively, while the neck region is the warmest part. The difference between the highest and lowest temperatures is 13.4°C. One can also notice that the average skin temperature dropped significantly compared to the neutral conditions.

**Table 2. Skin temperature distribution in cold environment [15].**

Segment	Skin temperature (°C)
Forehead	30.7
Cheek	27.7
Front neck	33.5
Back neck	34.5
Chest	30.9
Back	32.4
Abdomen	28.7
Upper arm	24.7
Lower arm	27.3
Hand	23.1
Left finger	21.1
Thigh	27.0
Shin	26.5
Calf	24.3
Foot	21.4
Average	26.8

Compared to cold surroundings, fingers and feet turned to be the warmest regions in a warm environment (Table 3). The skin temperature is evenly distributed in the upper body. The lower body is slightly cooler due to less activity than the upper body in the seated position. The maximum skin temperature difference between body parts is only 2.7°C.

**Table 3. Skin temperature distribution in warm environment [15].**

Segment	Skin temperature (°C)
Forehead	36.5
Cheek	36.3
Front neck	36.8
Back neck	36.1
Chest	36.1
Back	36.3
Abdomen	36.2
Upper arm	36.4
Lower arm	36.1
Hand	36
Left finger	36.7
Thigh	35.6
Shin	34.4
Calf	34.1
Foot	36.4
Average	35.8

## 2.2. Thermal comfort

The definition of thermal comfort is described as "the condition of the mind in which satisfaction is expressed with the thermal environment" in the American Society of Heating, Refrigerating and Air-Conditioning Engineers (ASHRAE) standard [20]. It is indeed a cognitive process, and psychological, physical, and physiological states affect the perception of thermal comfort [21]. Each person perceives thermal comfort differently, even in the same environment. Comfort can be achieved when occupants are within a specific temperature range, the moisture on the skin surface is low, and the physiological efforts for thermal regulations are reduced. Six factors are influencing thermal comfort; two of them are personal (activity level, clothing insulation), and the rest are physical (air velocity, air temperature, mean radiant temperature, and relative humidity) [21]. Thermal comfort is responsible for a productive and healthy workplace. The establishment of thermal comfort is also linked to energy consumption and contributes to building sustainability.

The necessity in energy consumption reduction for thermal comfort is becoming attractive. Therefore, for its assessment, different indices, experiments, surveys, models are being established. International comfort standards are built on these findings. In thermal comfort evaluation, professionals refer to standards that guarantee that at least 80% of people will be satisfied with thermal sensation [22]. There are major international comfort standards known as ASHRAE, ISO (International Standards Organization), and EN (European Standards). These standards provide well-defined temperature ranges for comfort, which are based on mathematical formulations derived by Fanger and are independent of race, sex, and age.

Fanger obtained comfort equations by substituting two linear equations obtained through experiments into heat balance equations [23]. He found that only two physiological factors: mean skin temperature and perspiration rate, were dependent on activity level. College-aged students participated in Fanger's experiments and were wearing the same clothes. From experimental data, linear equations from perspiration rate and activity level relation were developed. The linear relationship between mean skin temperature and activity level was derived from other experiments that involved different activity levels. The comfort equation was complemented further from data obtained from a bigger experiment [24]. ASHRAE adopted the equations and connected them to the 7-point scale Predicted Mean Vote (PMV) and Predicted Percentage Dissatisfied (PPD) indexes. In some experimental studies, ASHRAE's 7-point scale ranging from -3 (cold) to +3 (hot) was implemented [25]. Thermal

comfort or neutral condition corresponds to 0 among the range. The range is also applicable for CFD analysis.

Besides Fanger's model, there is Pierce two-node model [26]. The model uses two concentric cylinders, which represent the human body. The outer cylinder uses the skin surface temperature of 33.1°C, while the inner cylinder has the body core temperature of 37.1°C [21]. It should be noted that the two-node model is used for transient or physiological responses, while the PMV-PPD indexes are used only for steady-state situations [21].

Researchers from the Center for the Built Environment based in Berkley university created an online thermal comfort calculator [27]. The calculator is based on three major thermal comfort standards ISO 7730, EN 16798-1 and ASHRAE 55. Evaluations can be done by inserting five values which are the operative temperature, air speed, relative humidity, metabolic rate and clothing level. According to the ASHRAE 55 standard, the air speed is evaluated by averaging speed values at ankle (0.1 m), waist (0.6 m) and head (1.1 m) levels for seated occupants. "The operative temperature to can be defined as the average of the mean radiant and ambient air temperatures, weighted by their respective heat transfer coefficients" [28].

### **2.3. Mechanical ventilation**

Ventilation of building spaces plays a massive role in occupants' comfort and air quality [29]. There are two ventilation strategies used commonly in buildings: displacement and mixing ventilation [30, 31]. In 1899 Boyle Son et al. illustrated the systematic application of mixing ventilation [29]. In mixing ventilation, the incoming fresh air at high speed ( $> 1$  m/s) is supplied at the upper part of a room or ceiling. The primary purpose of mixing ventilation is to dilute the contaminated air in the room with fresh air at high velocities. A good mixing ventilation system should provide a uniform temperature and CO<sub>2</sub> particle distribution throughout the room [32]. Numerous experimental and numerical investigations were done to understand and improve mixing ventilation performance [33-35]. Findings and different positions of inlets and outlets are summarized in Table 4 (Appendix A). A practical handbook published by REHVA [36] gives a comprehensive description of the mixing ventilation applications.

As its name says, displacement ventilation uses fresh air to displace old air in the room. It is used exclusively for cooling. The air is supplied from the lower region of space closer to the floor with low velocity ( $< 0.5$  m/s). The temperature difference between the room and supply air is usually 2 - 4°C [37]. This inlet's position creates an upward movement of the air

as it gets warmer by heating sources (equipment, person, etc.) which results in stratified temperature and velocity profiles. Titus suggests minimizing the furniture with a cubical shape to facilitate the circulation of the flow [38]. John does not recommend supply airspeeds more than 0.25 m/s to avoid thermal discomfort [39]. However, thermal discomfort may still be present due to a draught or vertical temperature difference within 3°C for sitting and 4°C for standing occupants [40]. Like for mixing ventilation, many numerical and experimental studies were conducted for displacement ventilation described in Table 5 (Appendix A). Inlet, and outlet position is important because it was reported that mixing and displacement ventilation with the same airflow rate provide different degrees of air quality and thermal comfort [41, 42]. Advantages of displacement ventilation over mixing ventilation include better thermal comfort and air distribution, low operational cost, and noise. The main benefit is that displacement ventilation saves energy consumption by 43% [37]. However, displacement ventilation suffers from some shortcomings. The low air supply momentum cannot always be in balance with buoyancy forces, and in some cases, the buoyancy forces take over, leading to poor ventilation efficiency [30]. According to European standards [43], displacement ventilation should be used in spaces with a height of at least 2.7 m, while REHVA recommends using displacement ventilation in spaces that are higher than 3 m [44]. Another limitation is that it only can be used in cooling mode. Therefore, impinging jet ventilation (IJV) was proposed by Karimipannah and Awbi to eliminate the limitations of displacement ventilation [45].

The working principle of IJV is similar to displacement ventilation. The difference is in the air distribution method. Impinging jets are typically placed in the corner of the room with a small nozzle to floor distance. Emitted air at high velocity hits the floor and spreads along the floor, creating a thin layer that further rises toward the ceiling, causing stratification. This cool air compared to displacement ventilation can overpower the buoyancy force due to high momentum and better thermal comfort. IJV can also be utilized for room heating. IJV should be meticulously designed because the air supplied from floor level may cause high vertical temperature difference and draft [46].

#### **2.4. Human geometry in CFD**

In the computation domain, human geometry may have various shapes and positions. Mainly three positions are used: laying, sitting, and standing. No standard exists for human geometry in CFD; however, in many works done, human body surface size was between 1.594 m<sup>2</sup> and 1.688 m<sup>2</sup> [47]. The level of details on the human geometry depends on the problem's complexity. For simple cases, the body can be built from a cylinder [48], rectangle [49], and

cube [50], available in any CAD software. In more sophisticated cases, highly detailed geometry is required. The most recent approach is to use a 3D scanner to create a natural person's exact copy [51]. This way, one can obtain accurate results that are close to practical. However, this comes with a high computational cost. Highly detailed geometries require a significant amount of rectangular elements to mesh. For example, Sorensen et al. [51] had to use more than 1,000,000 triangular elements to discretize only the human surface. The body surface temperature in CFD studies usually is between 31°C [51] and 33.7°C [52]. It was also observed that the local airflow around an occupant is affected by its geometry while the global flow is not affected [47].

## **2.5. Impinging jets**

Impinging jets are devices that efficiently transfer mass or energy and are mainly used in industry. The high transfer of energy or mass is achieved by a pressurized gaseous or liquid flow directed on a target. Applications of impinging jets include cooling of electronic components, turbine blades and metals, defrosting of machinery components, defogging of glass surfaces, textile drying and many others. In surface cooling, impinging jets perform three times better than traditional confined flow cooling parallel to the surface, because the jets create a thinner boundary layer and cooling is facilitated by turbulence. The efficiency of impinging jets can further be enhanced by two orders of magnitude with pre-knowledge of the required heat transfer coefficient. Larger surfaces can be covered with multiple jets.

Impinging jet cooling is not efficient in cases: 1) when the impinging distance increases. This usually happens in work with moving highly non-uniform surfaces. It was found that a large jet nozzle to target distance leads to the loss of kinetic energy and reduction Nusselt number. 2) when the impinging distance is too small. Small distances block the possibility of uniform mass or heat transfer over a target. Implementation and construction of such jets may not be practical, especially when the jet velocity is high.

In the design of impinging jets, the heat transfer is evaluated by the Nusselt number, while the mass transfer is measured by the Schmidt number.

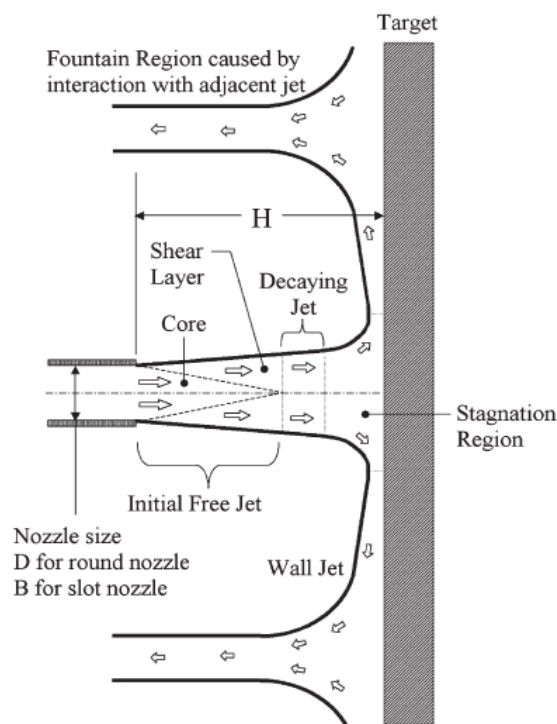
### **2.5.1. Impinging jet regions**

The exiting flow from impinging jets goes through several regions as depicted in Figure 1. The jet nozzle type defines turbulence characteristics of the flow. There are two common nozzle shapes of impinging jets – circular and slot. Circular jets have an axisymmetric flow

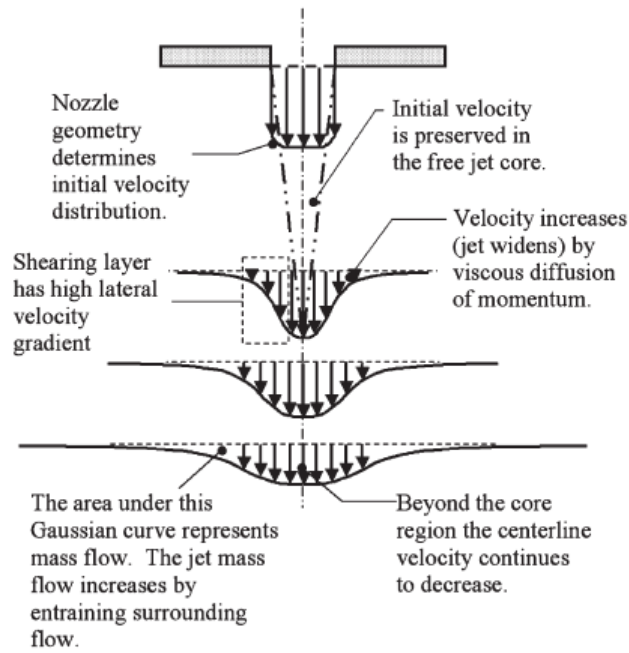
profile and develop turbulence in the upstream region. Compared to the circular jets, the flow in slot jets is less turbulent and has a two – dimensional profile.

The first region the flow passes through is called the free jet region. The region itself is divided in two: core and shear layer. The initial flow velocity remains constant in its core. Along the way, the flow starts to widen. This happens due to the shear layer formation by the velocity gradients at the jet edges which transfers momentum outwards. As a result, the flow loses its energy and the velocity profile widens.

The decaying jet area develops at four to eight jet diameters as the shear layer starts to expand in the direction of the jet center. The velocity profile in the decaying area has a shape similar to the Gaussian curve that continues to flatten and widen as the distance from jet nozzle increases (Figure 2). Flattening represents the decrease of the velocity at the jet center. Viskanta et al. [53] split the zone in two regions: developing and fully developed region. The initial velocity profile is present in the developing zone, while the profile transforms into the Gaussian form in the fully developed zone. Martin et al. [54] derived mathematical formulations based on the low Reynolds number for velocity predictions in the decaying jet region.



**Figure 1. Impinging jet flow regions [55]**



**Figure 2. Jet flow velocity profile [55]**

At the stagnation region the flow hits the target surface and turns away. The turning flow is nonuniform and is greatly affected by shear and normal stresses. This causes the stretching of the flow vortices and enhance the turbulence. Typically the stagnation region starts 1.2 jet diameters above the impingement surface [54]. The turned flow further enters the wall jet region and moves parallel to the target.

### 2.5.2. Turbulence generation and effects

The flow behavior can be predicted and categorized by the Reynolds number:

$$Re = \frac{UD}{\nu} \quad (2)$$

where  $U$  is the average velocity,  $D$  is the jet opening diameter and  $\nu$  is viscosity. The use of diameter  $D$  is correlated to the circular jets. For slot jets, two slot widths  $2B$  has to be used in evaluations. Depending on the Reynolds number, the flow categorization is as follow [53]:

- laminar  $Re < 1000$
- transitioning  $1000 < Re < 3000$
- turbulent  $Re > 3000$

For laminar flow analytical solutions can be found, however such flow provides much less heat transfer compared to turbulent flow. Turbulence greatly impacts the heat transfer, therefore most of the studies were done on turbulent impinging jets. For instance, a circular jet



with  $Re = 2000$  and  $H/D$  of 6 resulted in a Nusselt number of 19. The same jet with  $Re = 100,000$  was more efficient and had a Nusselt number of 212 [54]. Typically, laminar jets with small nozzle to target distance provide a Nusselt number in the range of 2–20.

Impinging jets used in industry usually operate at  $4000 < Re < 80,000$  and have  $H/D$  ratio between 2 and 12. The efficiency of jets depends on the distance  $H$  between the jet opening and the target, because the Nusselt number increases with  $H$  decrease. In the design of jets, one should aim for the optimum  $H$  distance, consider the type of jets, physical constraints, manufacturing possibilities and then adjust the jet diameter  $D$ . For small scale industry applications, commonly jets with diameters of 0.2 – 2 mm are used, while diameters between 5 – 30 mm are typical for large scale applications.

Mathematical representations of turbulent flow are based on mass, momentum, and energy conservation laws [55]:

$$\frac{\partial \bar{u}_i}{\partial x_i} = 0 \quad (3)$$

$$\rho \frac{\partial \bar{u}_i}{\partial t} + \rho \bar{u}_i \frac{\partial \bar{u}_j}{\partial x_j} = - \frac{\partial \bar{p}}{\partial x_i} + \frac{\partial \sigma_{ij}}{\partial x_j} + \frac{\partial \tau_{ij}}{\partial x_j} \quad (4)$$

$$\begin{aligned} \rho \frac{\partial \bar{u}_i}{\partial t} + \rho \bar{u}_i \frac{\partial \bar{u}_j}{\partial x_j} = & - \frac{\partial \bar{p}}{\partial x_i} + \frac{\partial}{\partial x_j} \left[ \mu \left( \frac{\partial \bar{u}_i}{\partial x_j} + \frac{\partial \bar{u}_j}{\partial x_i} \right) \right] \\ & + \frac{\partial}{\partial x_j} (-\rho \overline{u'_i u'_j}) \end{aligned} \quad (5)$$

$$\begin{aligned} \rho c_p \frac{\partial \bar{T}}{\partial t} + \rho c_p \bar{u}_j \frac{\partial \bar{T}}{\partial x_j} = & \sigma_{ij} \frac{\partial \bar{u}_i}{\partial x_j} + \frac{\partial}{\partial x_j} \left( \frac{\mu c_p}{Pr} \frac{\partial \bar{T}}{\partial x_j} \right) + \frac{\partial}{\partial x_j} (-\rho c_p \overline{u'_j T'}) \\ & + \mu \overline{\left( \frac{\partial u'_i}{\partial x_j} + \frac{\partial u'_j}{\partial x_i} \right) \frac{\partial u'_i}{\partial x_j}} \end{aligned} \quad (6)$$

$$\sigma_{ij} = \mu \left( \frac{\partial \bar{u}_i}{\partial x_j} + \frac{\partial \bar{u}_j}{\partial x_i} \right) \quad (7)$$

$$\tau_{ij} = -\rho \overline{u'_i u'_j} \quad (8)$$

Single variables with overbar stand for time-averages terms, fluctuating values are represented by a prime symbol, while correlation is represented by a large overbar.

In the time variant momentum expression, the second moment is adjusted to obtain the equation for Reynolds stresses [56]:

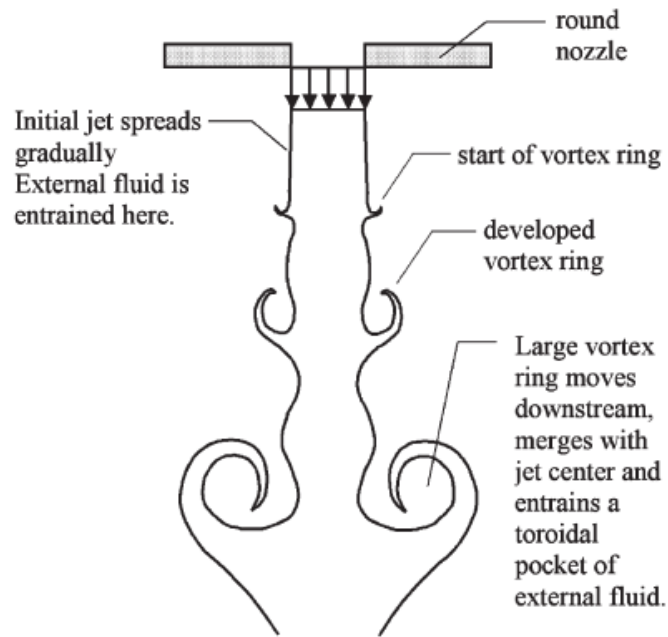
$$\begin{aligned}
\frac{\partial \tau_{ij}}{\partial t} + \bar{u}_k \frac{\partial \tau_{ij}}{\partial x_k} &= \left[ -\tau_{ik} \frac{\partial \bar{u}_j}{\partial x_k} - \tau_{jk} \frac{\partial \bar{u}_i}{\partial x_k} \right] + \left[ \frac{p'}{\rho} \left( \frac{\partial u'_i}{\partial x_j} + \frac{\partial u'_j}{\partial x_i} \right) \right] \\
\text{Convective transport} \quad \text{Turbulence production} \quad \text{Pressure-strain rate} \\
&+ \left[ \frac{\partial}{\partial x_k} \left( -\overline{u'_i u'_j u'_k} - \frac{p'}{\rho} \{u'_i \delta_{jk} + u'_j \delta_{ik}\} \right) \right] \\
&\quad \text{Turbulent diffusion gradient} \\
&+ \left[ -2\nu \frac{\partial u'_i}{\partial x_k} \frac{\partial u'_j}{\partial x_k} \right] + \left[ \nu \frac{\partial^2 \tau_{ij}}{\partial x_k \partial x_k} \right] \\
&\quad \text{Turbulent dissipation} \quad \text{Molecular diffusion}
\end{aligned} \tag{9}$$

$k$  represents the specific turbulent kinetic energy and is correlated with the turbulence intensity. To make its units nondimensional, a velocity ratio is taken in which the denominator term is the time-averaged kinetic energy:

$$Tu = \sqrt{\frac{\overline{u'_i u'_i}}{\bar{u}_i \bar{u}_i}} \tag{10}$$

Turbulence formation can be forced by installing obstacles (e.g, tabs, screens) in the pipe flow or at the jet opening. This is done to enhance the heat transfer coefficient. A previous study showed that this approach shortens the jet core region and increases a Nusselt number because of the H/D ratio decrease [57].

In the jet flow, the appearance of turbulence may already start at the initial jet zone. The shear layer is the source of turbulence generation that creates instability of the flow. The velocity profile and the location of the shear layer can create flow oscillations that move from side to side. Along the way, these oscillations may evolve into large-scale eddies and may have sizes equal to or larger than the jet diameter. Then, they either get interfered by other flow features or naturally split into smaller eddies. Graphical representation of vortex formation is shown in Figure 3.



**Figure 3. Turbulence formation in jets [55]**

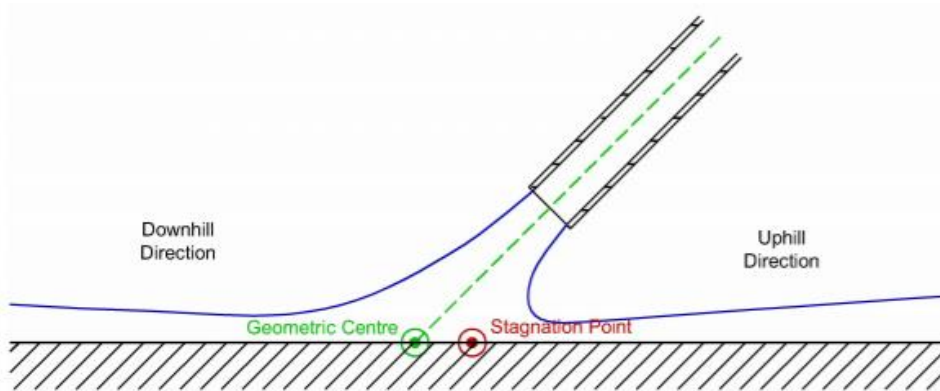
Turbulence in smaller scales can also be produced in the decaying region because, in that area, the shear layer stretches across the jet center. The flow at the jet center may form turbulent pockets and small eddies that eventually turn into an unstructured turbulent flow field.

In the stagnation region, the promotion of turbulence happens due to normal strains and stresses caused by the deceleration of the flow. Investigations done by Abe and Suga [58] revealed that the heat and mass transfer is dominated by eddies of large scale in the stagnation region.

The presence of turbulence enhances the heat transfer ratio. Flow eddies facilitate the mixing of fluids with different temperatures and kinetic energy. This important property allows to increase the local heat transfer by penetrating and removing the boundary layer.

Ashforth-Frost et al. assessed the nozzle geometry's influence on the potential core length [59]. In the investigation, semi-confined and unconfined jets with the fully developed and flat flow were used. The findings reveal that the potential core zone can be extended by 7% with the fully developed flow. For flat velocity profiles, the shear is higher, leading to the early penetration to the center of the jet. Authors also report that for the semi-confinement jets, the potential core can be extended by 20%.

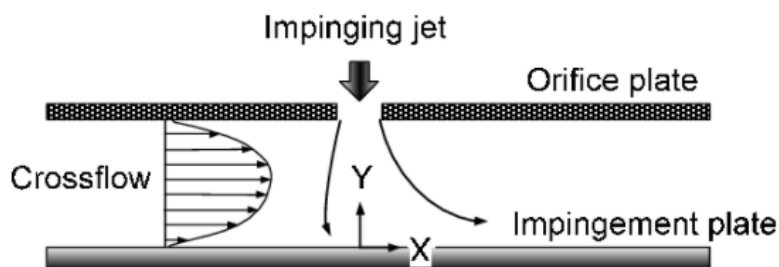
In Figure 4, configurations of inclined impinging jets are represented. The geometric center is the jet centerline's intersection with the target surface. The flow deflected by the impingement plate is split into downhill and uphill zones. Compared to the jets' perpendicular position, the stagnation point is slightly shifted towards the uphill direction for oblique jets.



**Figure 4. Flow characteristics of oblique jets**

Observations by Foss et al. for inclined impinging jets at an angle of  $9^\circ$  showed that the stagnation point's position in relation to the geometric center was shifted further than maximum static pressure [60]. Another investigation conducted by Foss et al. for  $45^\circ$  of impingement angle showed the coincidence of the stagnation point and maximum static pressure [61]. Goldstein et al. also conducted studies on impinging jets with varying angles from  $30^\circ$  to  $60^\circ$  [62]. It can be concluded that the highest heat transfer for oblique impingement does not happen at the geometric center.

Confinement changes the heat transfer rate of impinging jets. The air impinged from a nozzle plate is known as semi-confined. Further expansion of the nozzle plate length only increases the jet's confinement. In electronics cooling, confinement cannot be avoided due to small and restricted spaces. Single and conjugate impingement is used in the cooling of electronics. Crossflow, as demonstrated in Figure 5, occurs with confinement and should be taken into account because confinement is determined by the direction and magnitude of the crossflow. Crossflow impact on the heat transfer rate can be seen in works done by Goldstein et al. [63]. Comparison studies on the flow characteristics of conjugate and single jet were also published by Goldstein et al. [64]. Crossflow formation due to confinement was investigated by Obot et al. [65].



**Figure 5. Crossflow in confined space**

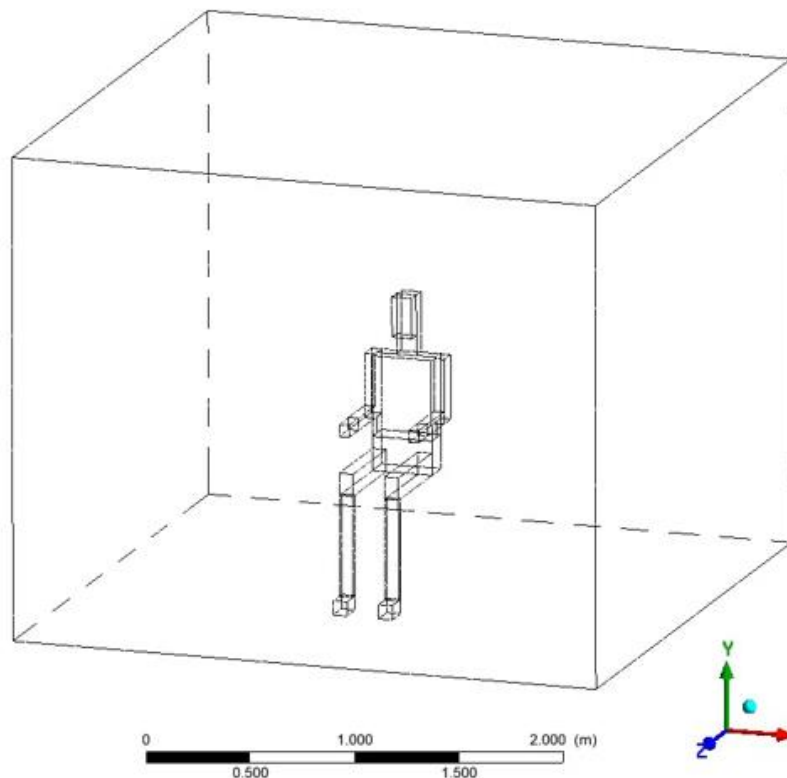
## Chapter 3 – Methodology

### 3.1. Domain preparation (Verification and Validation)

Dimensions of our computational domain were taken from Sørensen et al. [51]. In Sørensen et al.'s work, the computational manikin was an exact 3D scanned copy of a woman. Authors report that a considerable amount of mesh elements on the 3D scanned occupant's surface must capture the heat flux gradients. The use of complicated geometries requires high computational effort. Therefore, it was decided to simplify the occupant's shape. The person's overall geometry was simple, made from cubes, and divided into 16 parts (arms, legs, etc.) to evaluate temperature distribution at each part.

Mesh verification and model validation were the first steps in preparing the computational domain. Ansys CFX module was used for these purposes. The validated model was used for further simulations to find out the best-suited flow and jets characteristics. The thermal comfort was assessed by the CBE comfort tool.

The computational domain has a shape of a box with dimensions of 2.95 (length) x 2.95 (width) x 2.4 (height). The domain was filled with air from which the Boolean command subtracted a person. The occupant's feet are not in contact with the floor and are 0.02 m above. The occupant's face center coincides with the room center (Figure 6).



*Figure 6. Computational domain*

The governing equations for CFD are listed below.

Continuity equation:

$$\frac{D\rho}{Dt} + \rho \frac{\partial U_i}{\partial x_i} = 0 \quad (11)$$

Momentum equation:

$$\rho \frac{\partial U_j}{\partial t} + \rho U_i \frac{\partial U_j}{\partial x_i} = -\frac{\partial P}{\partial x_j} - \frac{\partial \tau_{ij}}{\partial x_i} + \rho g_j \quad (12)$$

where,

$$\tau_{ij} = -\mu \left( \frac{\partial U_j}{\partial x_i} + \frac{\partial U_i}{\partial x_j} \right) + \frac{2}{3} \delta_{ij} \mu \frac{\partial U_k}{\partial x_k} \quad (13)$$

Energy equation:

$$\rho c_\mu \frac{\partial T}{\partial t} + \rho c_\mu U_i \frac{\partial T}{\partial x_i} = -P \frac{\partial U_i}{\partial x_i} + \lambda \frac{\partial^2 T}{\partial x_i^2} - \tau_{ij} \frac{\partial U_j}{\partial x_i} \quad (14)$$

For validation purposes, three the most popular two equations turbulence models Standard k- $\epsilon$ , Standard k- $\omega$  and Shear Stress Transport were tested. Mathematical expressions and constant coefficients for each model are represented below.

Standard k- $\epsilon$  equations:

$$\frac{\partial(\rho k)}{\partial t} + \text{div}(\rho k U) = \text{div} \left[ \frac{\mu_t}{\sigma_k} \text{grad } k \right] + 2\mu_t S_{ij} \cdot S_{ij} - \rho \epsilon \quad (15)$$

$$\frac{\partial(\rho \epsilon)}{\partial t} + \text{div}(\rho \epsilon U) = \text{div} \left[ \frac{\mu_t}{\sigma_\epsilon} \text{grad } \epsilon \right] + C_{1\epsilon} \frac{\epsilon}{k} 2\mu_t S_{ij} \cdot S_{ij} - C_{2\epsilon} \rho \frac{\epsilon^2}{k} \quad (16)$$

Rate of change of $k$ or $\epsilon$	Transport of $k$ or $\epsilon$ by convection	Transport of $k$ or $\epsilon$ by diffusion	Rate of production of $k$ or $\epsilon$	Rate of destruction of $k$ or $\epsilon$
---	--	---	---	--

$$C_\mu = 0.09 \quad \sigma_k = 1.00 \quad \sigma_\epsilon = 1.30 \quad C_{1\epsilon} = 1.44 \quad C_{2\epsilon} = 1.92$$

Standard k- $\omega$  equations:

$$\frac{\partial(\rho k)}{\partial t} + \text{div}(\rho k U) = \text{div} \left[ \left( \mu + \frac{\mu_t}{\sigma_k} \right) \text{grad } k \right] + P_k - \beta^* \rho k \omega \quad (17)$$

$$P_k = \left( 2\mu_t S_{ij} \cdot S_{ij} - \frac{2}{3} \rho k \frac{\partial U_i}{\partial x_j} \delta_{ij} \right) \quad (18)$$

$$\begin{aligned}
\frac{\partial(\rho\omega)}{\partial t} + \text{div}(\rho\omega U) &= \text{div} \left[ \left( \mu + \frac{\mu_t}{\sigma_\omega} \right) \text{grad } \omega \right] \\
\text{Rate of change of } k \text{ or } \omega & \quad \text{Transport of } k \text{ or } \omega \text{ by convection} & \quad \text{Transport of } k \text{ or } \omega \text{ by diffusion} \\
+ \gamma_1 \left( 2\rho S_{ij} \cdot S_{ij} - \frac{2}{3} \rho \omega \frac{\partial U_i}{\partial x_j} \delta_{ij} \right) - \beta_1 \rho \omega^2 & \\
& \quad \text{Rate of production of } k \text{ or } \omega & \quad \text{Rate of dissipation of } k \text{ or } \omega
\end{aligned} \tag{19}$$

$$\sigma_k = 2.0 \quad \sigma_\omega = 2.0 \quad \gamma_1 = 0.553 \quad \beta_1 = 0.075 \quad \beta^* = 0.09$$

Shear Stress Transport equations:

$$\frac{\partial(\rho k)}{\partial t} + \text{div}(\rho k U) = \text{div} \left[ \left( \mu + \frac{\mu_t}{\sigma_k} \right) \text{grad } k \right] + P_k - \beta^* \rho k \omega \tag{20}$$

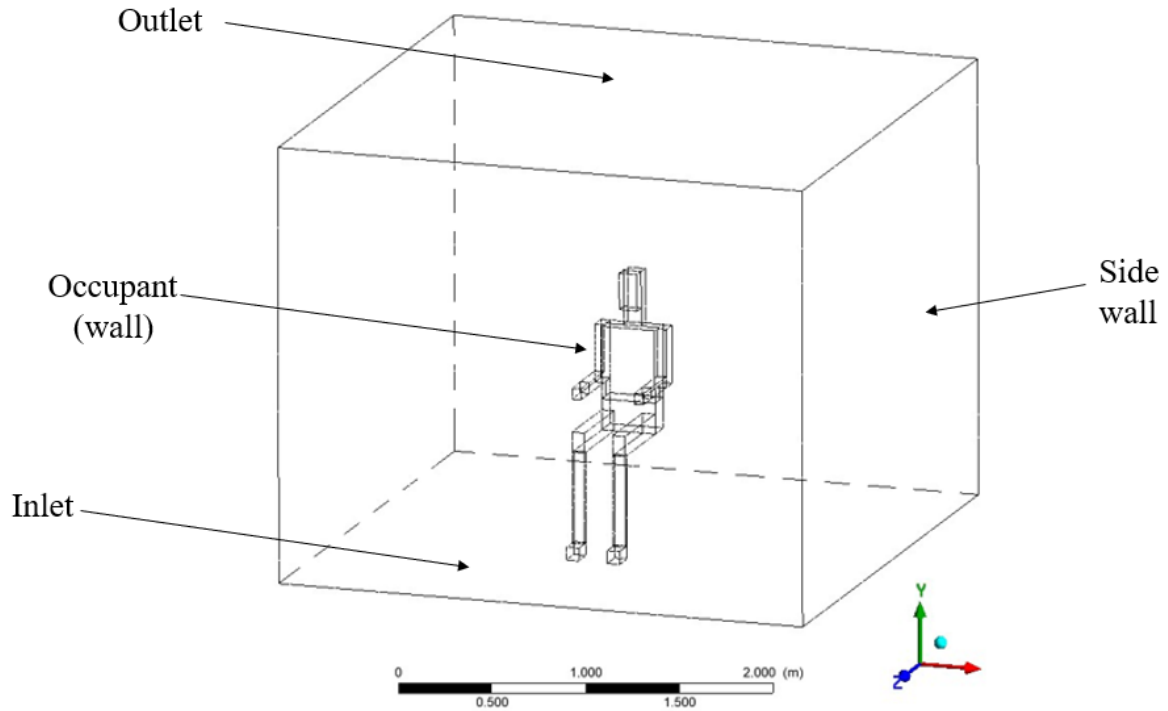
$$\begin{aligned}
\frac{\partial(\rho\omega)}{\partial t} + \text{div}(\rho\omega U) &= \text{div} \left[ \left( \mu + \frac{\mu_t}{\sigma_{\omega,1}} \right) \text{grad } \omega \right] \\
+ \gamma_2 \left( 2\rho S_{ij} \cdot S_{ij} - \frac{2}{3} \rho \omega \frac{\partial U_i}{\partial x_j} \delta_{ij} \right) - \beta_2 \rho \omega^2 + 2 \frac{\rho}{\sigma_{\omega,2} \omega} \frac{\partial k}{\partial x_k} \frac{\partial \omega}{\partial x_k} & \\
\end{aligned} \tag{21}$$

$$\sigma_k = 1.0 \quad \sigma_{\omega,1} = 2.0 \quad \sigma_{\omega,2} = 1.17 \quad \gamma_2 = 0.44 \quad \beta_2 = 0.083 \quad \beta^* = 0.09$$

Blending functions are introduced to the last, cross-diffusion term, for transitions between the k- $\epsilon$  and k- $\omega$  models:

$$C = F_C C_1 + (1 - F_C) C_2 \tag{22}$$

Surfaces of the computational domain need to be specified by giving names for which boundary conditions were set exactly as described by Sørensen et al. [51] (Figure 7). All the walls of the domain were given no-slip condition. The air is supplied from the floor with 0.02 m/s speed, 19.75°C temperature, 30% turbulence fractional intensity with a 0.004 m turbulence eddy length scale. Outlet covered the whole ceiling with relative pressure of 0 Pa. Human surface had a fixed temperature of 31°C while the four sidewalls of the room were at 19.75°C. Radiation was considered in the simulations for the whole human body and sidewall, emissivity values were defined a 0.95 and 1.00, respectively.



**Figure 7. Named selections of the domain**

The domain was divided into tetrahedral elements with multiple mesh refinements on the human surface and the cylindrical area from the head to the ceiling. The room was refined to capture the temperature values accurately. The addition of inflation layers and mesh refinement of the occupant surface was done for heat flux evaluation. The wall  $y^+$  value was set to be 0.97 and 2.63 for Standard  $k-\epsilon$  and Standard  $k-\omega$ /SST models, respectively. The Finite Volume Method was utilized for the solution and discretization of the governing equations for each grid cell. The mesh verification study summary is presented in Table 6 and Table 7. The temperature root mean square (RMS) error was calculated from 10 points of data equally distributed on a line from head to the ceiling. Mesh 3 (Figure 8) was the final mesh as it satisfied the error criteria ( $< 1\%$ ) with 338446 nodes.

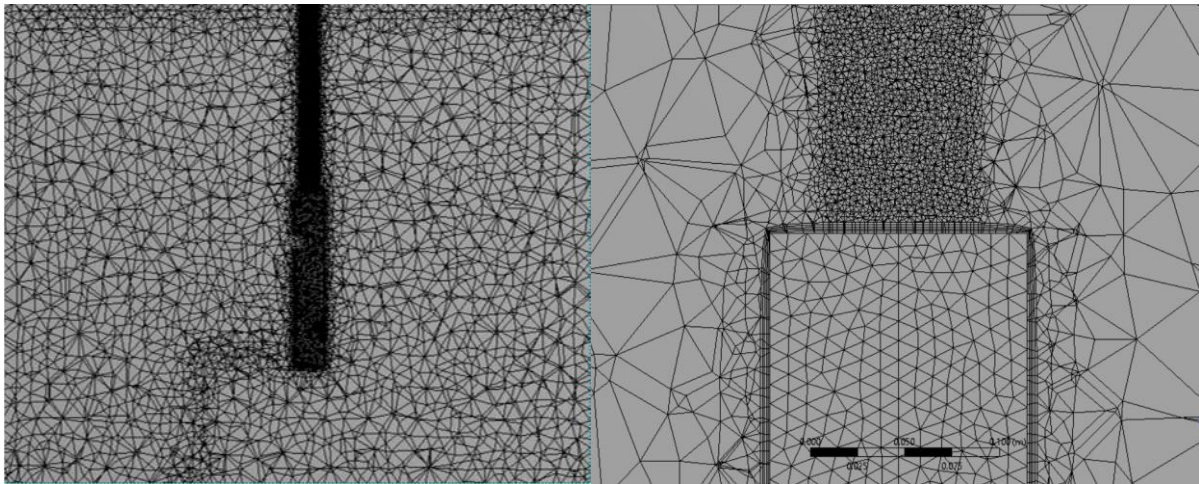
**Table 6. Mesh comparison**

	Mesh 1	Mesh 2	Mesh 3	Mesh 4
Heat Flux ( $\text{W}/\text{m}^2$ )	67.0584	67.4448	-	-
Temperature at 1.98 m ( $^{\circ}\text{C}$ )	294.84198	294.850159	294.845276	294.849274



**Table 7. Error between meshes**

	Mesh 2 vs. Mesh 1	Mesh 3 vs. Mesh 2	Mesh 4 vs. Mesh 3
Heat Flux (%)	0.57	-	-
Temperature at 1.98 m (%)	0.003	0.002	0.001
Temperature RMS (%)	1.86	1.97	0.71

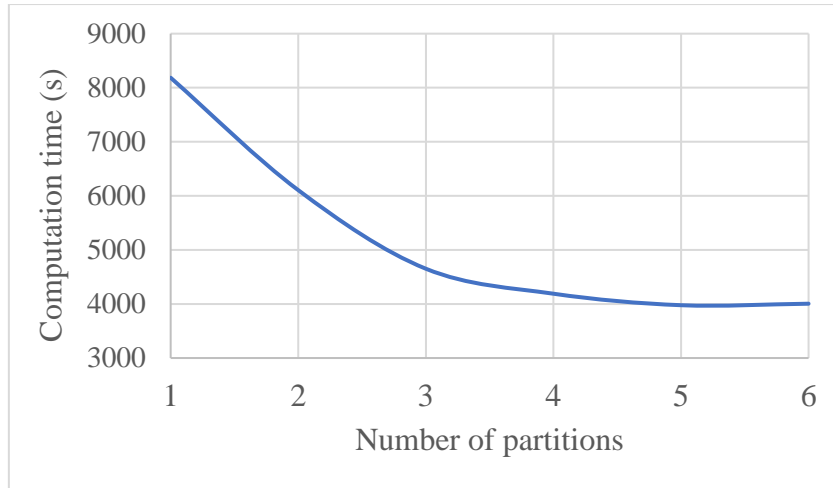


**Figure 8. Final mesh representation at  $x = 1.475\text{ m}$**

The computational time was recorded (Table 8) and plotted (Figure 9) for different partitions to ensure the CPU's optimum usage. Calculations were done on a computer with Intel Core i7 – 8700 @ 3.20 GHz and 16 Gb RAM. The addition of partitions after five does not produce significant improvement in time.

**Table 8. Time is taken by the different number of partitions**

Number of partitions	Time
1	2 hrs 16 min 23.728 s
2	1 hrs 41 min 45.129 s
3	1 hrs 17 min 32.200 s
4	1 hrs 09 min 49.747 s
5	1 hrs 06 min 16.963 s
6	1 hrs 06 min 44.887 s



**Figure 9. Computational time vs. Number of partitions graph**

The total time spent for simulations in combinations with different radiation and turbulence models is summarized in Table 9.

**Table 9. Simulation time for different turbulence and radiation models**

<b>Turbulence model + Radiation model</b>	<b>Time</b>
k-e + Discrete Transfer	1 hrs 09 min 18.020 s
k-e + Monte Carlo	1 hrs 15 min 42.527 s
k-w + Discrete Transfer	2 hrs 13 min 02.491 s
k-w + Monte Carlo	2 hrs 27 min 12.571 s
SST + Discrete Transfer	2 hrs 28 min 45.840 s
SST + Monte Carlo	2 hrs 32 min 41.686 s

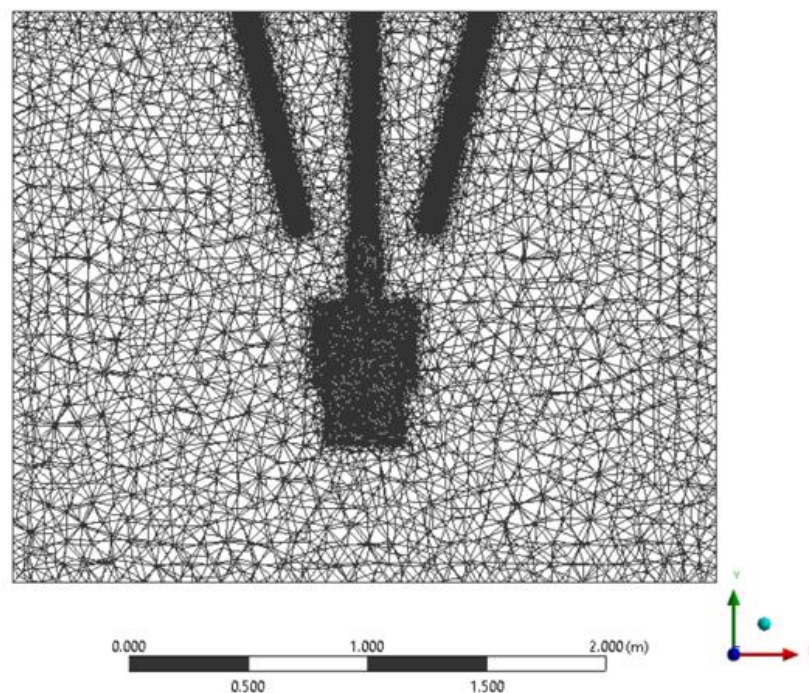
For validation, air velocity above the head and body heat flux values were compared with the experimental data. Experimental values for the heat flux and velocity are 88.26 W/m<sup>2</sup> and above 0.5 m/s, respectively. Comparison of different turbulence and radiation models revealed that the combination of SST and Monte Carlo models produced the lowest error of 4.34% (Table 10), which is in the 10% range. The error could be caused due to the use of simplified human geometry.

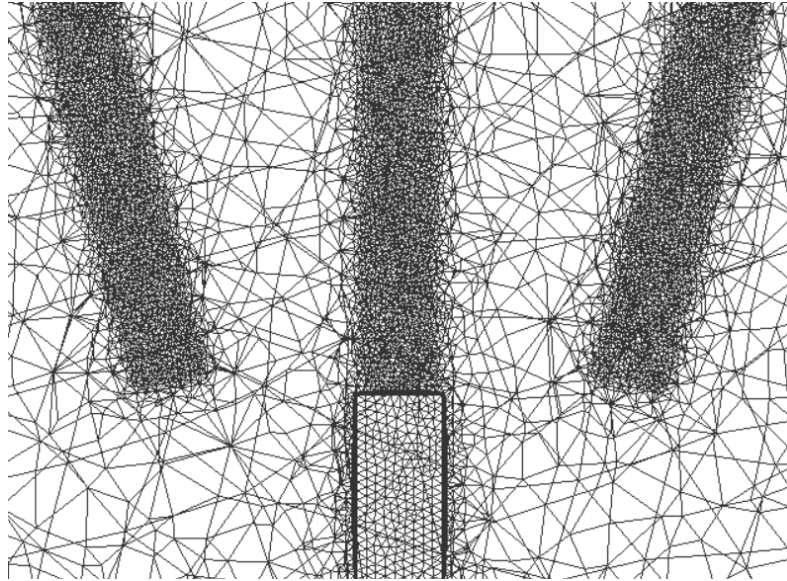
**Table 10. Validation of the model**

<b>Turbulence model + Radiation model</b>	<b>Heat Flux (W/m<sup>2</sup>)</b>	<b>Velocity (m/s)</b>	<b>Error (%)</b>
k-e + Discrete Transfer	67.06	0.34	24.02
k-e + Monte Carlo	72.85	0.34	17.46
k-w + Discrete Transfer	96.25	0.57	9.05
k-w + Monte Carlo	94.01	0.57	6.51
SST + Discrete Transfer	96.23	0.57	9.03
SST + Monte Carlo	92.09	0.57	4.34

### 3.2. Mesh verification for jets

Mesh verification study was performed to capture velocity values produced by cylindrical jets. Initially, mesh was verified for the jet normal to the occupant, then copied to other jets. At each mesh refinement, velocity values at two locations were checked. The first location is the middle point of the cylinder axis. The second one, is a line parallel to the axis lying on the cylinder outer surface with length half of the cylinder height. The line contained ten uniformly distributed velocity values. Mesh independence was achieved after three refinements as represented in Table 11 and Table 12. The final mesh contained 1,283,771 elements (Figure 10).





**Figure 10. Mesh at  $z = 1.407\text{ m}$**

**Table 11. Mesh independence study for jets**

	Mesh 1	Mesh 2	Mesh 3	Mesh 4
Velocity at cylinder axis center (m/s)	4.92	4.96	4.98	4.99

**Table 12. Error between meshes for jets**

	Mesh 2 vs. Mesh 1	Mesh 3 vs. Mesh 2	Mesh 4 vs. Mesh 3
Velocity at the middle of the cylinder axis (%)	0.81	0.40	0.20
Velocity RMS at the reference line (%)	7.34	2.17	0.73

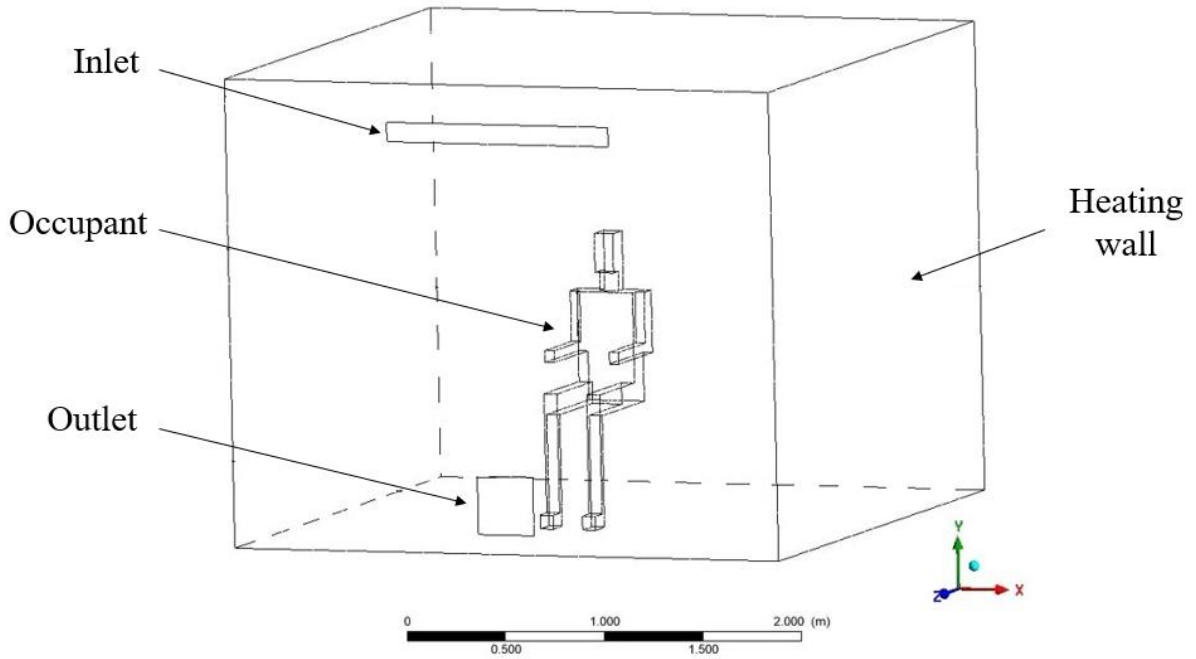
## Chapter 4 – Results and Discussion

### 4.1. Base case scenario (mixing ventilation cooling)

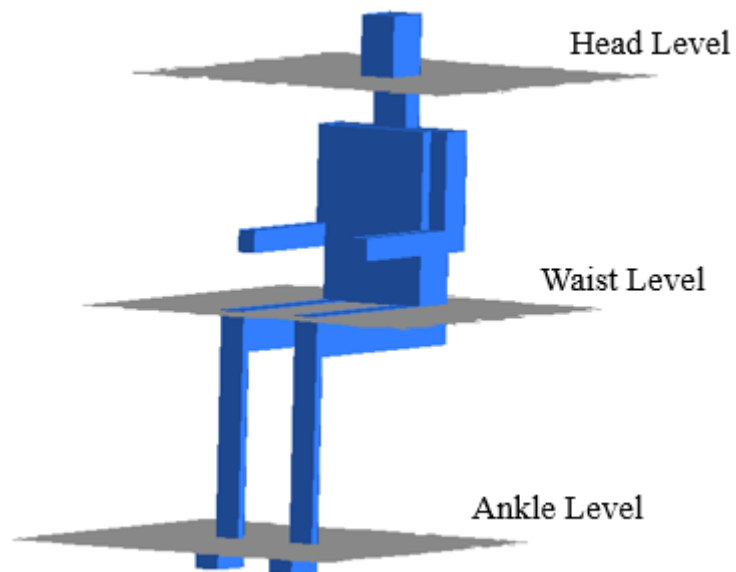
For the base case scenario, the boundary conditions, inlet and outlet dimensions were taken from the work done by Yang et al. [66]. The air was supplied from the upper zone of the room and extracted from the lower region as illustrated in Figure 11. The inlet and outlet had dimensions of 1.2 m (length) x 0.1 m (width) and 0.3 m x 0.3 m respectively. All the walls, except the wall on the right were assumed to be adiabatic. The right wall represented the outdoor temperature in summer and was set to have a constant temperature of 35°C.

The required inlet air parameters that create a thermal comfort were obtained from numerous simulations. A significant energy imbalance and its fluctuations were present during simulations. It was fixed by initialization of the energy results and adjusting the timescale factor. Initialization was performed by switching the inlet and outlet boundary conditions to wall type, so pure conduction case could run. Obtained results were used as initial conditions for actual simulations. Velocity components imbalances were less than 0.05 %, while energy imbalance was lower than 3 %.

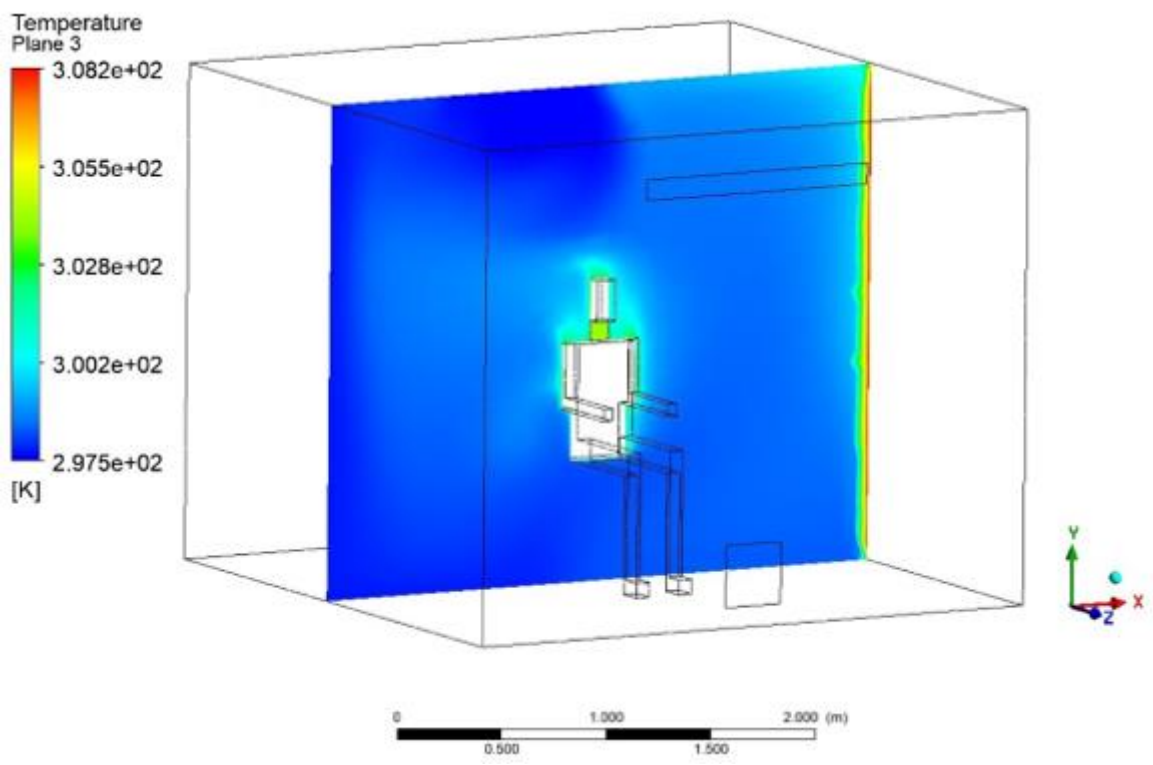
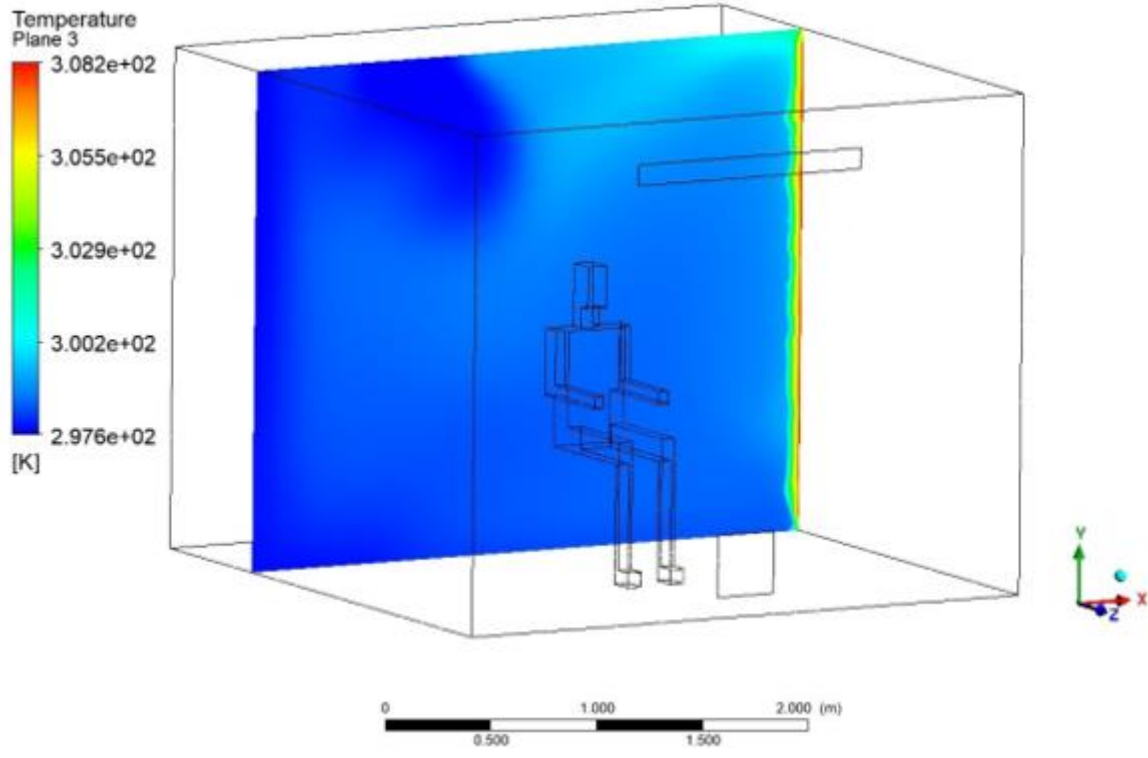
It was found that the inlet velocity of 1.1 m/s at 24°C provides thermal comfort for the occupant in the room under assumptions that the person is wearing a summer cloth (0.5 clo) and the relative humidity is 50 %. The PMV and PPD values were found to be - 0.35 and 8% respectively. One of the comfort evaluation parameters – air speed was calculated by averaging the velocity results from three planes, each with dimensions of 0.5 m x 0.5 m (Figure 12). It was found to be 0.14 m/s. According to the ASHRAE 55 standard, the location of these planes is at 0.1 m (ankle level), 0,6 m (waist level) and 1.1 m (head level) for seated occupants. The room temperature was equal to 25.4°C and its distribution was very uniform as expected from mixing ventilation (Figure 13).

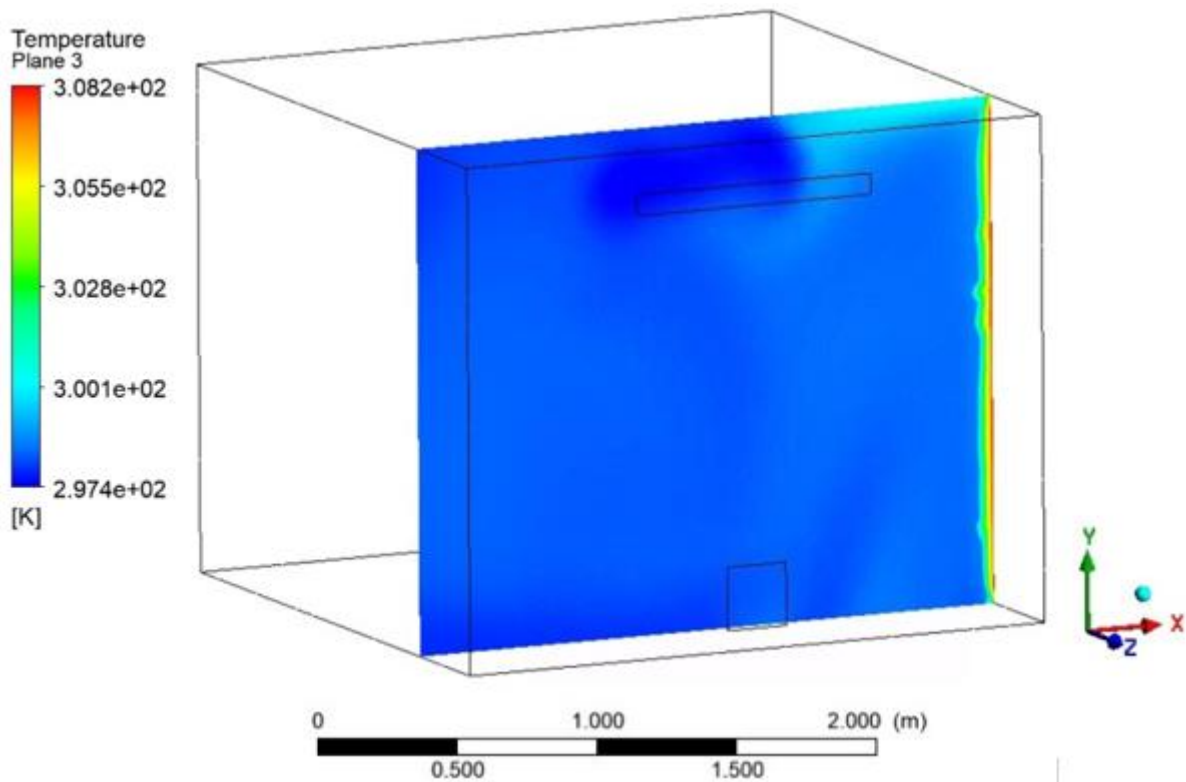


*Figure 11. Domain for the base case scenario*



*Figure 12. Planes at head (1.1 m), waist (0,6 m) and ankle levels (0.1 m)*





*Figure 13. Room temperature distribution at a)  $z = 0.8\text{ m}$  b)  $z = 1.407\text{ m}$  c)  $z = 2.4\text{ m}$*

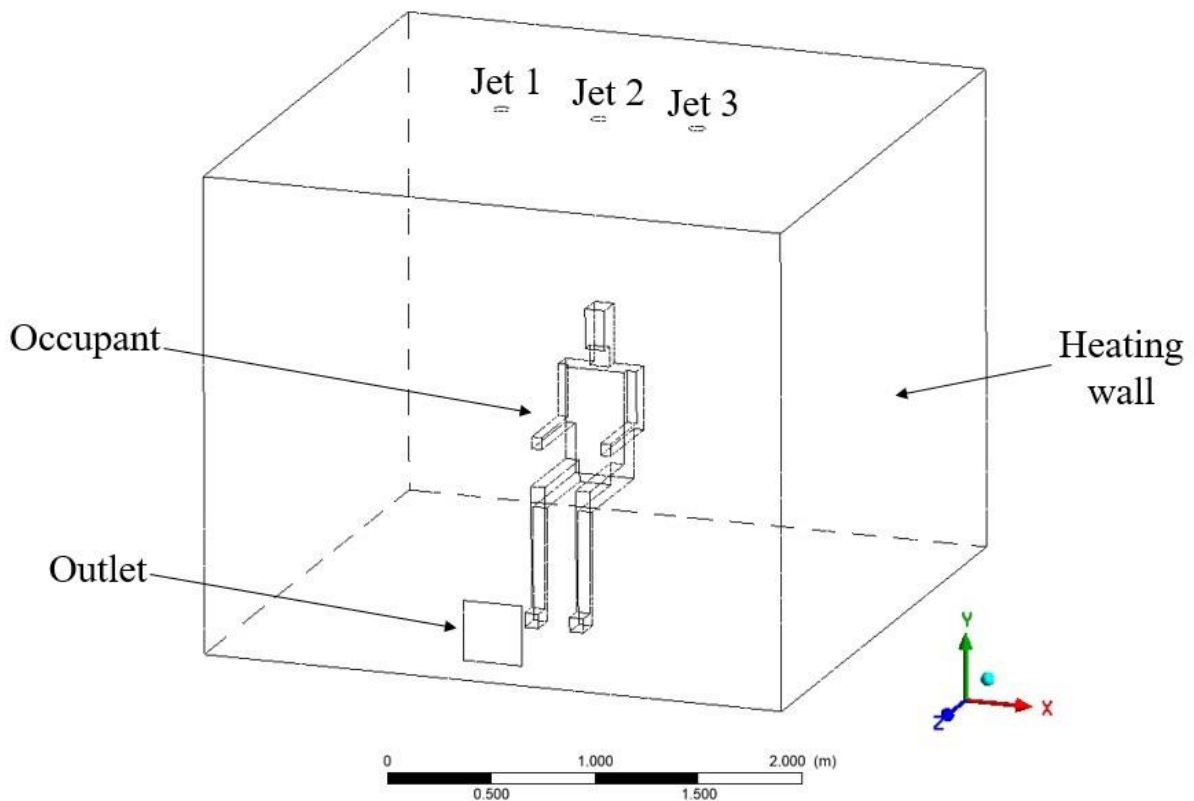
#### 4.2. Cooling with impinging jets

Direct occupant cooling was implemented by impinging jets mounted on the ceiling. For energy consumption comparison between the base case and impinging jets, the jets' inlet temperature retained at  $24^{\circ}\text{C}$  and outlet position was not changed. The diameter of cylindrical impinging jets was calculated from the H/D ratio, where H is the distance between Jet 2 and the occupant's head. This distance is equal to 0.94 m and was considered to be optimal. In reality, the occupant may want to stand up and stretch. If the distance was small, the occupant could hit the jets and damage himself and/or the jets. Common jet diameters used in large industry applications (5 – 30 mm) are not suitable for this case, because they result in a small H distance. Since the H/D ratio should be equal to a value between 2 and 12, the smallest jet diameter for cooling the occupant was found to be 8 cm.

The performance of Jet 2 alone was tested. The mass flow of one jet was not enough to provide thermal comfort to the occupant. Therefore, two additional jets were installed 0.5 m apart from Jet 2 (Figure 14) and directed to the head ( $64^{\circ}$  angle), shoulders ( $76^{\circ}$  angle) and waist ( $80^{\circ}$  angle). All three jets had the same velocity. Simulation results show that at an inlet



velocity of 2 m/s thermal comfort is achieved regardless of angle. A summary of average air speed at each angle can be seen in Table 13.



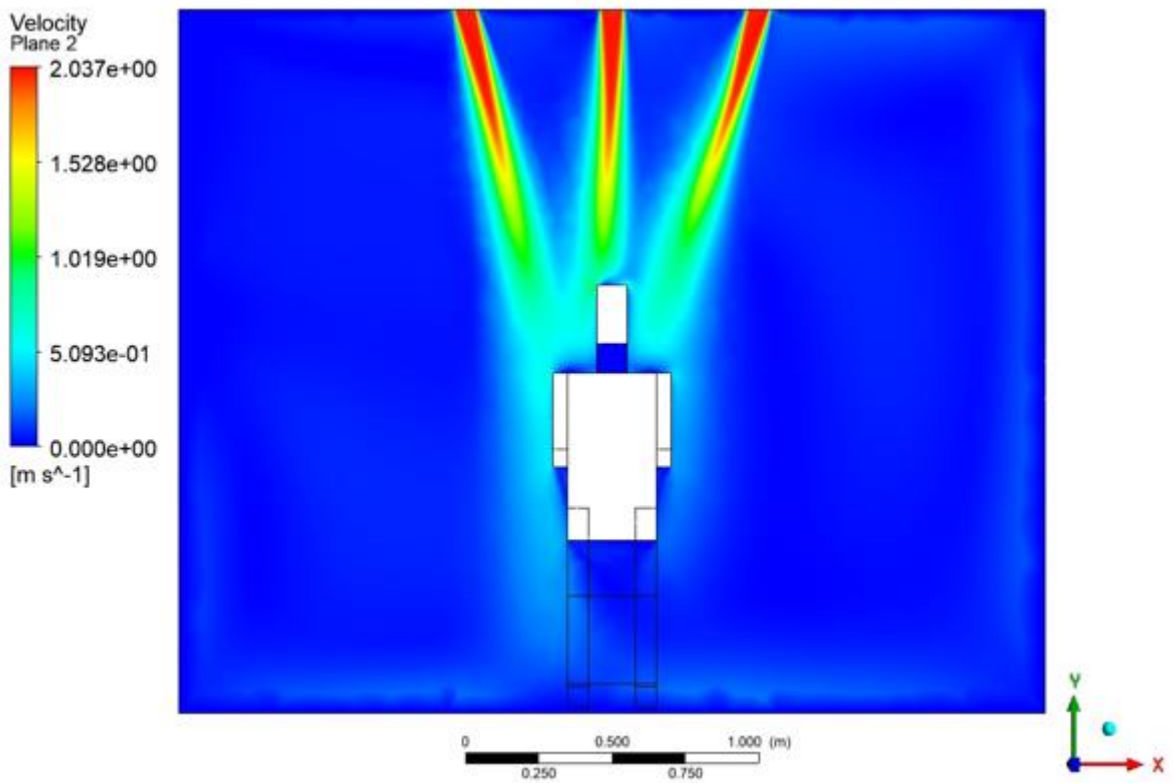
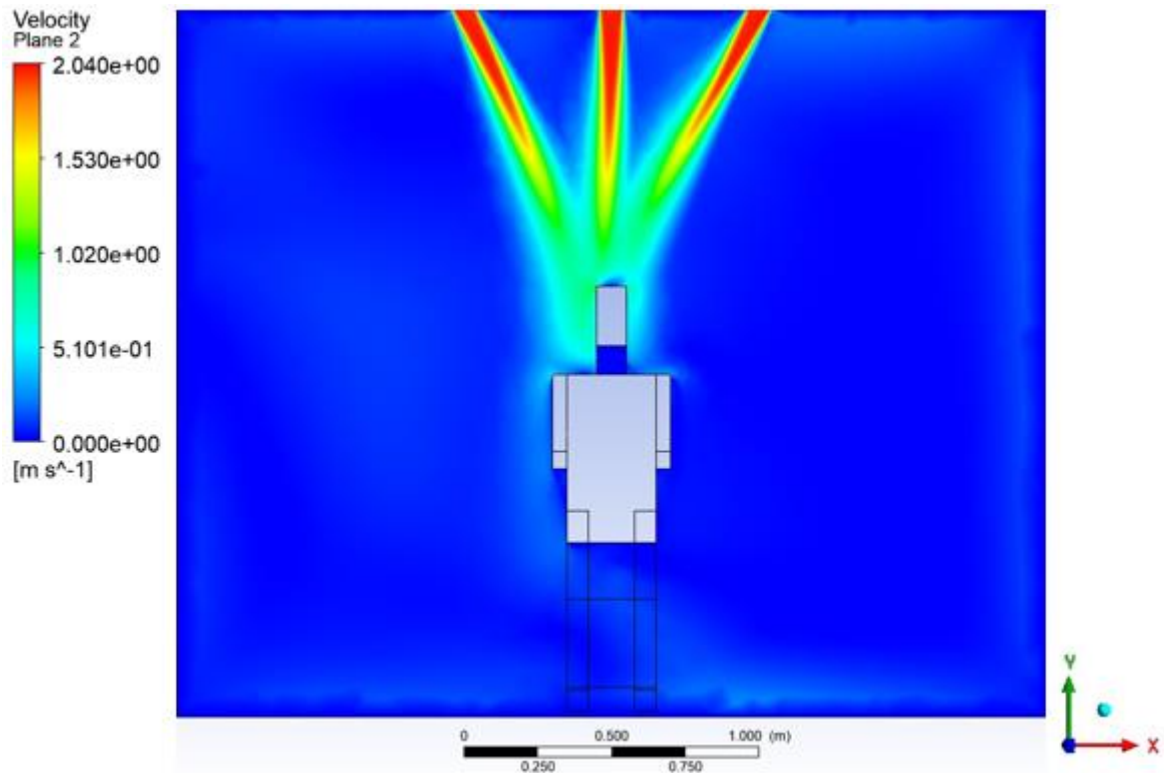
**Figure 14. Room with three jets**

**Table 13. Summary of average air speed at each angle**

Speed Angle	Head level speed (m/s)	Waist level speed (m/s)	Ankle level speed (m/s)	Average air speed (m/s)
64°	0.30	0.16	0.14	0.2
76°	0.24	0.20	0.15	0.2
80°	0.22	0.16	0.14	0.17

The PMV and PPD indexes for the head and shoulders cases were 0.37 and 8%, and 0.48 and 10% for the waist case. Directed cooling of the head or shoulders provides slightly better comfort than cooling the waist region.

Velocity profiles at different impinging angles can be seen in Figure 15.



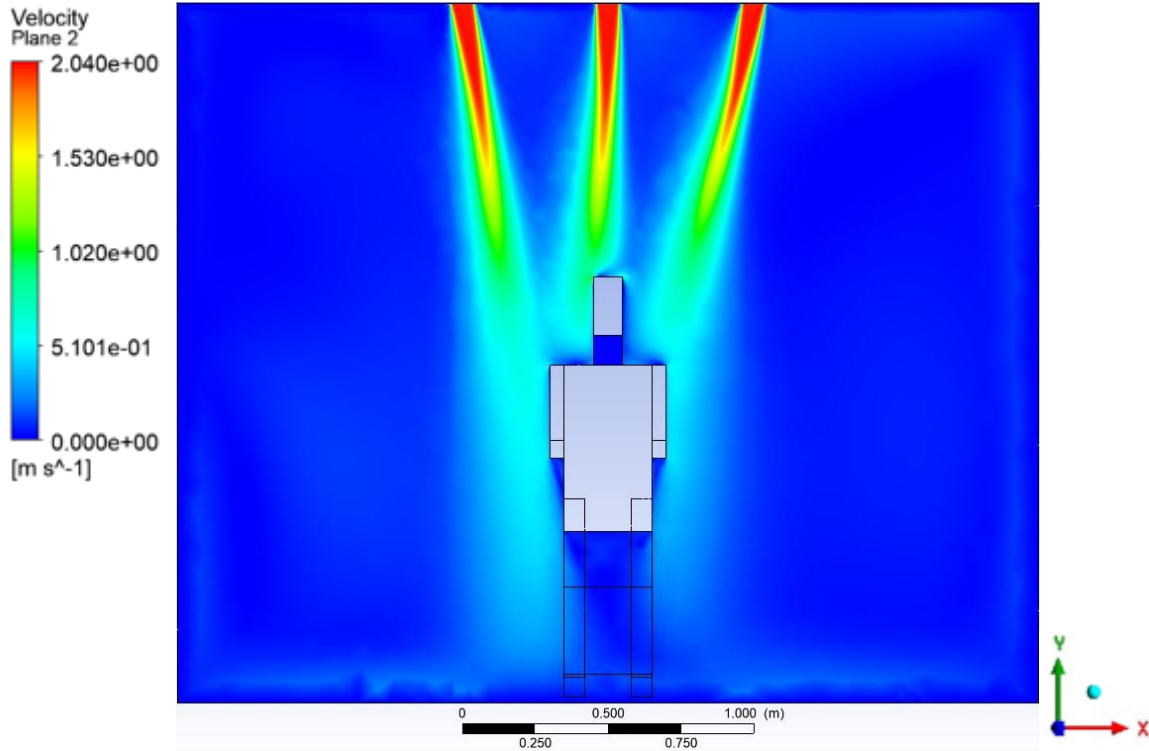


Figure 13. Jet velocity profiles at a) 64° b) 76° c) 80°

### 4.3. Energy consumption comparison

The energy spent for cooling was calculated using the following formula [67]:

$$\dot{Q} = \sum \dot{m}_0 h_0 - \sum \dot{m}_i h_i \quad (23)$$

where  $\dot{m}_0$  and  $\dot{m}_i$  are the mass flow rates at outlet and inlet,  $h_0$  and  $h_i$  are the enthalpies at outlet and inlet.

Ansys CFX, by default, uses the reference value for enthalpy of 0 J/kg at 25°C. Negative enthalpy values mean that the air temperature is less than the reference value.

Since the mass flow for both cooling cases is the same at the inlet and outlet, eq. (23) can be rewritten as:

$$\dot{Q} = \dot{m}(h_0 - h_i) \quad (24)$$

Below, energy consumption calculations are shown for each case:

$$\dot{Q}_{base\ case} = 0.16 \cdot (-48.72 + 1004.41) \approx 153\ W \quad (25)$$

$$\dot{Q}_{jets} = 0.035 \cdot (2562.41 + 1004.41) \approx 125\ W \quad (26)$$

Cooling with impinging jets is more efficient and allows to save 18.3% of energy compared to traditional cooling.

## Chapter 5 – Conclusion

Traditional cooling methods waste energy by cooling the entire space. In the era of global energy crisis and global warming, it is necessary to find energy efficient solutions. Impinging jets have been widely used in small and large industrial applications as efficient cooling sources. Therefore, this work was dedicated to see if impinging jets can be used as an energy efficient alternative for space cooling that at the same time could provide comfort to the occupants. The approach was to cut electricity consumption by targeted cooling of an occupant. Numerical investigations were done over a validated domain with dimensions of 2.95 m x 2.95 m x 2.4 m (height) with a person sitting in the center. The outdoor temperature of 35°C represented summer conditions. The boundary conditions that provide comfort in traditional cooling were imposed on the case with impinging jets. One cylindrical impinging jet with a diameter of 8 cm located on the ceiling and normal to the person could not provide thermal comfort due to mass flow rate deficiency. However, three impinging jets with an inlet velocity of 2 m/s and the same diameter were enough to achieve comfort regardless of the directed angle. Energy consumption comparison between traditional and jet cooling revealed that the use of impinging jets is able to save 18.3% of energy. The percentage could be increased by an extensive parametric optimization which might be the basis for future work.

## References

- [1] Santamouris, M., & Kolokotsa, D. (2015). On the impact of urban overheating and extreme climatic conditions on housing, energy, comfort and environmental quality of vulnerable population in Europe. *Energy and Buildings*, 98, 125-133.
- [2] Pitarma, R., Marques, G., & Ferreira, B. R. (2017). Monitoring indoor air quality for enhanced occupational health. *Journal of medical systems*, 41(2), 1-8.
- [3] Seppänen, O. A., & Fisk, W. (2006). Some quantitative relations between indoor environmental quality and work performance or health. *Hvac&R Research*, 12(4), 957-973.
- [4] Tsai, D. H., Lin, J. S., & Chan, C. C. (2012). Office workers' sick building syndrome and indoor carbon dioxide concentrations. *Journal of occupational and environmental hygiene*, 9(5), 345-351.
- [5] Lan, L., Wargocki, P., Wyon, D. P., & Lian, Z. (2011). Effects of thermal discomfort in an office on perceived air quality, SBS symptoms, physiological responses, and human performance. *Indoor Air*, 21, 376-390.
- [6] Zhang, S., Lin, Z., Zhou, P., & Cheng, Y. (2019). Fully mixed air model based cooling load estimation method for both stratum ventilation and displacement ventilation. *Energy and Buildings*, 199, 247-263.
- [7] IEA (2018), The Future of Cooling, IEA, Paris <https://www.iea.org/reports/the-future-of-cooling>
- [8] Santamouris, M. (2016). Cooling the buildings—past, present and future. *Energy and Buildings*, 128, 617-638.
- [9] Levine, M., D. Ürge-Vorsatz, K. Blok, L. Geng, D. Harvey, S. Lang, G. Levermore, A. Mongameli Mehlwana, S. Mirasgedis, A. Novikova, J. Rilling, H. Yoshino, 2007: Residential and commercial buildings. In *Climate Change 2007: Mitigation. Contribution of Working Group III to the Fourth Assessment Report of the Intergovernmental Panel on Climate Change* [B. Metz, O.R. Davidson, P.R. Bosch, R. Dave, L.A. Meyer (eds)], Cambridge University Press, Cambridge, United Kingdom and New York, NY, USA.
- [10] IEA (2020), Cooling, IEA, Paris <https://www.iea.org/reports/cooling>
- [11] Biddle, J. (2008). Explaining the spread of residential air conditioning, 1955–1980. *Explorations in Economic History*, 45(4), 402-423
- [12] Fell, D., & Cornish-Bowden, A. (1997). *Understanding the control of metabolism* (Vol. 2). London: Portland press.
- [13] Djongyang, N., Tchinda, R., & Njomo, D. (2010). Thermal comfort: A review paper. *Renewable and sustainable energy reviews*, 14(9), 2626-2640.
- [14] Zingano BW. A discussion on thermal comfort with reference to bath water temperature to deduce a midpoint of the thermal comfort temperature zone. *Renewable Energy* 2001;23:41–7.
- [15] Arens, E. A., & Zhang, H. (2006). The skin's role in human thermoregulation and comfort.
- [16] Romanovsky, A. A. (2014). Skin temperature: its role in thermoregulation. *Acta physiologica*, 210(3), 498-507.
- [17] DuBois, D., & DuBois, E. F. (1915). Fifth paper the measurement of the surface area of man. *Archives of Internal Medicine*, 15(5\_2), 868-881.
- [18] Zhang, H. (2003). Human thermal sensation and comfort in transient and non-uniform thermal environments.
- [19] Olesen, B. W., & Fanger, P. O. (1973). The skin temperature distribution for resting man in comfort. *Archives des sciences physiologiques*, 27(4), 385-393.
- [20] ASHRAE, S. (2017). Standard 55-2017, Thermal Environmental Conditions for Human Occupancy. Am. Soc. Heating, Refrig. Air-Conditioning Eng, Atlanta, USA.

- [21] Lin Z, Deng S. A study on the thermal comfort in sleeping environments in the subtropics—developing a thermal comfort model for sleeping environments. *Building and Environment* 2008;43:70–80.
- [22] Charles KE. Fanger’s Thermal Comfort and Draught Models. Institute for Research in Construction National Research Council of Canada, Ottawa, K1A 0R6, Canada IRC Research Report RR-162 October 10; 2003
- [23] Fanger PO. Calculation of thermal comfort: introduction of a basic comfort equation. *ASHRAE Transactions* 1967;73(2):III4.1–2.
- [24] Fanger PO. Thermal comfort, analysis and application in environmental engineering. Copenhagen: Danish Technical Press; 1970
- [25] Charles KE. Fanger’s Thermal Comfort and Draught Models. Institute for Research in Construction National Research Council of Canada, Ottawa, K1A 0R6, Canada IRC Research Report RR-162 October 10; 2003.
- [26] Gagge AP, Fobelets AP, Berglund LG. A standard predictive index of human response to the thermal environment. *ASHRAE Transactions* 1986;92(2B): 709–31.
- [27] Tartarini, F., Schiavon, S., Cheung, T., Hoyt, T., 2020. CBE Thermal Comfort Tool: online tool for thermal comfort calculations and visualizations. *SoftwareX* 12, 100563.
- [28] American Society of Heating, Refrigerating and Air-Conditioning Engineers. (2009). 2009 ASHRAE handbook: Fundamentals. Atlanta, GA: American Society of Heating, Refrigeration and Air-Conditioning Engineers.
- [29] Boyle & Son R. Natural and artificial methods of ventilation. London.1899.
- [30] Awbi HB (2003). *Ventilation of Buildings*. London: Taylor & Francis.
- [31] Heiselberg P (1996). Room air and contaminant distribution in mixing ventilation.
- [32] Awbi HB. Energy Efficient Ventilation for Retrofit Buildings. In *Proceedings of 48th AiCARR International Conference on Energy Performance of Existing Buildings*, 22–23 September 2011, Baveno, Italy, p. 23–46.
- [33] Harris E. *Ventilation in American Dwellings*. Viley & Halsted. 1858.
- [34] Billington NS, Roberts BM. *Building Services Engineering – A review of its development*. A. Wheaton & Co. Ltd., Exeter. 1892.
- [35] Butler WF. *Ventilation of buildings*. Van Nostrand Publisher, New York, 1873.
- [36] Müller D, Kandzia C, Kosonen R, Melikov AK, Nielsen PV. *Mixing Ventilation - Guidebook on mixing air distribution design*. REHVA Guidebook, No.19, 2013
- [37] Ren, S., Tian, S., & Meng, X. (2015, November). Comparison of displacement ventilation, mixing ventilation and underfloor air distribution system. In *2015 International Conference on Architectural, Civil and Hydraulics Engineering*. Atlantis Press.
- [38] Titus (2014). *Displacement Ventilation*. Available at [https://www.titushvac.com/docs/2014 catalog/displacement\\_2013.pdf](https://www.titushvac.com/docs/2014_catalog/displacement_2013.pdf). Accessed 1 Apr 2015.
- [39] John DA (2011). designing for comfort: Selecting air-distribution outlets. *ASHRAE Journal*, 53(9): 38–46.
- [40] ASHRAE, S. (2017). *Standard 55-2017, Thermal Environmental Conditions for Human Occupancy*. Am. Soc. Heating, Refrig. Air-Conditioning Eng, Atlanta, USA.
- [41] Kuo J-Y, Chung K-C (1999). The effect of diffuser’s location on thermal comfort analysis with different air distribution strategies. *Journal of Building Physics*, 22: 208–229.
- [42] Lin Z, Chow TT, Fong KF, Tsang CF, Wang Q (2005a). Comparison of performances of displacement and mixing ventilations. Part II: Indoor air quality. *International Journal of Refrigeration*, 28: 288–305
- [43] EDR (2015). *Design Brief: Displacement Ventilation 2.0*. In: *Energy Design Resources*. Available at <http://energydesignresources.com/resources/publications/design-briefs/design-brief-displacementventilation.aspx>. Accessed 1 Apr 2015.
- [44] REHVA Guidebook No. 23 - *Displacement Ventilation*. REHVA., 2017.

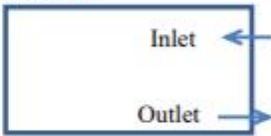
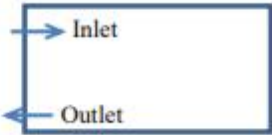
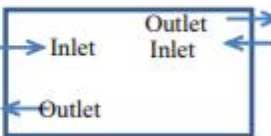

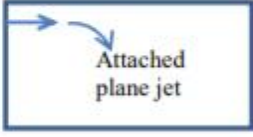
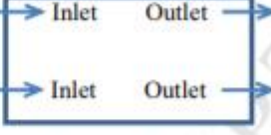
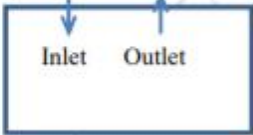
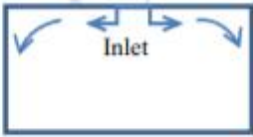
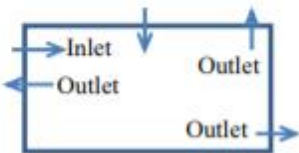
- [45] T. Karimipannah, H.B. Awbi. Theoretical and experimental investigation of impinging jet ventilation and comparison with wall displacement ventilation. *Building Environ*, 37 (2002), pp. 1329-1342
- [46] A.K. Melikov, G. Langkilde, B. Derbiszewski. Airflow characteristics in the occupied zone of rooms with displacement ventilation. *ASHRAE Trans*, 96 (1) (1990), pp. 555-563
- [47] Gao, N. P., & Niu, J. L. (2005). CFD study of the thermal environment around a human body: a review. *Indoor and built environment*, 14(1), 5-16.
- [48] Dunnett, S. J. (1994). 29. P. 06 A numerical study of the factors affecting worker exposure to contaminant. *Journal of Aerosol Science*, 25, 481-482.
- [49] Niwa, K., Murakami, S., Kato, S., Kondo, Y., & Kitamura, N. (1996). Numerical analysis of flow and temperature field with local air conditioning by supply jets from the seats in hall. In *Proceedings of ROOMVENT* (Vol. 96, pp. 307-314).
- [50] Heinsohn, R. J. (1991). *Industrial ventilation* (No. BOOK). J. Wiley.
- [51] Sørensen, D. N., & Voigt, L. K. (2003). Modelling flow and heat transfer around a seated human body by computational fluid dynamics. *Building and environment*, 38(6), 753-762.
- [52] Murakami, S., Zeng, J., & Hayashi, T. (1999). CFD analysis of wind environment around a human body. *Journal of Wind Engineering and Industrial Aerodynamics*, 83(1-3), 393-408.
- [53] Viskanta, R. (1993). Heat transfer to impinging isothermal gas and flame jets. *Exp. Thermal Fluid Sci.* 6, 111–134.
- [54] Martin, H. (1977). Heat and mass transfer between impinging gas jets and solid surfaces. *Adv. Heat Transfer* 13, 1–60.
- [55] Zuckerman, N., & Lior, N. (2006). Jet impingement heat transfer: physics, correlations, and numerical modeling. *Advances in heat transfer*, 39, 565-631.
- [56] Peyret, R. (1996). “*Handbook of Computational Fluid Mechanics*”. Academic Press, San Diego, CA.
- [57] Yoshida, H., Suenaga, K., and Echigo, R. (1990). Turbulence structure and heat transfer of a two-dimensional impinging jet with gas–solid suspensions. *Int. J. Heat Mass Transfer* 33, 859–867.
- [58] Abe, K. and Suga, K. (2001). Large eddy simulation of passive scalar in complex turbulence with flow impingement and flow separation. *Heat Transfer – Asian Res.* 30, 402-418.
- [59] Ashforth-Frost, S., and Jambunathan, K., 1996, “Effect of nozzle geometry and semi-confinement on the potential core of a turbulent axisymmetric free jet,” *International Communications in Heat and Mass Transfer*, 23, pp. 155 – 162.
- [60] Foss, J. F., and Kleis, S. J., 1976, “Mean flow characteristics for the oblique impingement of an axisymmetric jet,” *AIAA Journal*, 14, pp. 705 – 706.
- [61] Foss, J. F., 1979, “Measurement in a large-angle oblique jet impingement flow,” *AIAA Journal*, 17, pp. 801 – 802.
- [62] Goldstein, R. J., and Franchett, M. E., 1988, “Heat transfer from a flat surface to an oblique impinging jet,” *ASME Journal of Heat Transfer*, 110, pp. 84 – 90.
- [63] Goldstein, R. J., and Behbahani, A. I., 1982, “Impingement of a circular jet with and without cross flow,” *International Journal of Heat and Mass Transfer*, 25, pp. 1377 – 1382.
- [64] Goldstein, R. J., and Timmers, J. F., 1982, “Visualisation of heat transfer from arrays of impinging jets,” *International Journal of Heat and Mass Transfer*, 25, pp. 1857 – 1868.
- [65] Obot, N. T., and Trabold, T. A., 1987, “Impingement heat transfer within arrays of circular jets: Part 1 - effects of medium, intermediate, and complete crossflow for small and large spacings,” *ASME Journal of Heat Transfer*, 109, pp. 872 – 879.
- [66] Yang, L., & Ye, M. (2014). CFD simulation research on residential indoor air quality. *Science of the Total Environment*, 472, 1137-1144.

[67] Aryal, P., & Leephakpreeda, T. (2015). CFD analysis on thermal comfort and energy consumption effected by partitions in air-conditioned building. *Energy Procedia*, 79, 183-188.

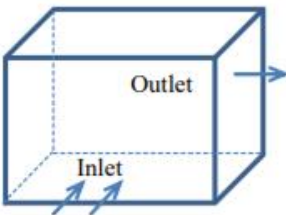
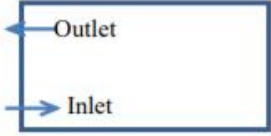
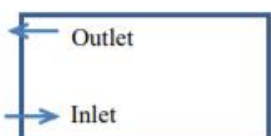
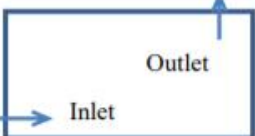
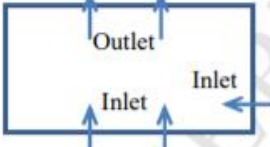


## Appendix A

**Table 4. A short summary of studies of mixing ventilation**

	Locations of airflow inlet and outlet	Methods	Main focus	Findings
Boyle Son (1899) [19]		Investigation	Airflow distribution and indoor air quality.	<ul style="list-style-type: none"> <li>This is one of the very earliest forms of mechanical ventilation</li> <li>Downdraught ventilation by mechanical impulsion is pronounced by public health experts to be highly prejudicial to health.</li> </ul>
Clements (1975) [14]		Model experiment	Airflow pattern and the effect of Archimedes number.	<ul style="list-style-type: none"> <li>The air pattern is almost a function of the Archimedes number. As <math>Ar</math> increases, the jet deflection from the horizontal increases.</li> </ul>
Sandberg et al. (1986) [25]		Experimental study	Air exchange efficiency and contaminant exposure.	<ul style="list-style-type: none"> <li>The ceiling-to-floor system gives rise to a comparatively rapid exchange of the air with heating. However, the evacuation of the contaminant is delayed.</li> </ul>
Nielsen (1991) [112]		Modeling and experimental study	Simplified design method.	<ul style="list-style-type: none"> <li>Simplified design models work well with simple geometry</li> <li>Measurements show significant deviation.</li> </ul>
Sandberg et al. (1992) [26]		Experimental study	The effect of Archimedes number on the airflow distribution.	<ul style="list-style-type: none"> <li>The critical supply Archimedes number at which the jet breaks away from the surface as soon as it leaves the nozzle was just below 0.03.</li> </ul>
Awbi and Gan (1993) [27]		Numerical study	Air distribution and ventilation effectiveness.	<ul style="list-style-type: none"> <li>Air distribution systems should be different for heating and cooling in order to achieve a comfortable room environment.</li> </ul>
Lee and Awbi (2004) [28]		Experimental and numerical study	The effects of partitions on the room air quality as well as ventilation performance.	<ul style="list-style-type: none"> <li>Increasing the partition gap underneath from 0%H to 10%H causes an overall improvement in the air change efficiency.</li> </ul>
Cao et al. (2010) [29]		Experimental study	Maximum velocity decay in the air distribution via attached plane jet.	<ul style="list-style-type: none"> <li>Attached plane jet can be used as an effective method to avoid draught in mixing ventilation conditions.</li> </ul>
Krajčik et al. (2012) [33]		Experimental study	Air distribution and ventilation effectiveness.	<ul style="list-style-type: none"> <li>The ventilation effectiveness varied between 0.4 and 1.2, where 1 is complete mixing, which depends on the position of air terminal devices.</li> </ul>

**Table 5. A summary of studies of displacement ventilation**

	Locations of airflow inlet and outlet	Methods	Main focus	Findings
Li et al. (1992) [34]		Experimental study	Temperature profile in a room.	<ul style="list-style-type: none"> <li>The vertical temperature profile is considerably affected by conduction through the wall and the radiative heat transfer between room surfaces, particularly between the ceiling and the floor.</li> </ul>
Awbi and Gan (1993) [27]		Numerical study	Air distribution and ventilation effectiveness.	<ul style="list-style-type: none"> <li>Displacement ventilation performs better than mixing ventilation in terms of ventilation effectiveness.</li> </ul>
Awbi (1998) [44]		Experimental and numerical study	Air distribution and ventilation effectiveness.	<ul style="list-style-type: none"> <li>Ventilation effectiveness for heat distribution for displacement ventilation is almost twice the value for mixing ventilation.</li> </ul>
Lee and Lam (2007) [41]		Numerical study	Temperature gradient and plume effect.	<ul style="list-style-type: none"> <li>The feasible zone capacity range diminished with decrease in design room temperature and/or room height.</li> </ul>
Lee et al. (2009) [45]		Experimental and numerical study	Airflow and contaminant distributions.	<ul style="list-style-type: none"> <li>The air distribution effectiveness seems to be proportional to the ceiling height.</li> </ul>